PREDICTING PULSATIONS AND SURGE IN MIXED RECIPROCATING AND CENTRIFUGAL COMPRESSOR PIPING SYSTEMS

A Thesis

by

JOHN VINCENT SHAW

Submitted to the Office of Graduate and Professional Studies of
Texas A&M University
in partial fulfillment of the requirements for the degree of

MASTER OF SCIENCE

Chair of Committee,	Alan Palazzolo
Committee Members,	Thomas Strganac
	Sivakumar Rathinam
Head of Department,	Andreas Polycarpou

December 2015

Major Subject: Mechanical Engineering

ABSTRACT

The purpose of this work is to develop a method for modelling centrifugal compressor surge in the presence of pressure pulsations in gas transmission lines, and examine the effects of pulsation amplitude and frequency on centrifugal compressor operating stability. Anecdotal field evidence suggests that it is possible for a centrifugal compressor to enter surge when pressure pulsations are present, even in the case where the centrifugal compressor would otherwise operate at a stable point. In such a situation it has been concluded that the instability results from the pulsations.

The method used for the model of the piping system is a finite element model of the pipe acoustics, with a reciprocating compressor model and a centrifugal compressor model as boundary conditions. The details of these models and the methods for coupling them are a large portion of this work. The combined centrifugal compressor and piping acoustic model are used in a variety of numerical experiments investigating the effect of pulsation amplitude and frequency on the operating point of the centrifugal compressor.

The results of the numerical experiments show that piping system acoustic properties have a strong effect on pulsation amplitude, and pulsations have a strong effect on compressor operating point. The pulsations cause an oscillation in operating point away from the compressor's steady state operating point. The effect is stronger as pulsation amplitude increases and as pulsation frequency approaches the natural frequency of the piping system. If the pulsations are strong enough, they can force the centrifugal compressor operating point over the surge limit, and then back into the stable operating region before the compressor enters a surge cycle. Numerical experiments show that the pulsations must push the centrifugal compressor over the surge limit and remain there long enough, if a surge cycle is to develop. Therefore, it is concluded that pulsations can cause a centrifugal compressor to cross the surge limit, and that larger pulsations will indeed cause surge when the operating point is across the surge limit for long enough.

ACKNOWLEDGEMENTS

Firstly, I would like to acknowledge Dr. Palazzolo for serving as my research advisor over the course of this project. His guidance and technical insight provided consistent direction and invaluable support. Next, a sincere thank you to Dr. Rathinam of the TAMU Mechanical Engineering department and Dr. Strganac of the TAMU Aerospace Engineering for their generosity in serving as members of my research committee. Also, a word of appreciation for the members and participants of the Turbomachinery Research Consortium for the funding contributed to this project.

Finally, to my wife, Kathleen, and children, Keira and Connor, for their unconditional support of my graduate school career and unwavering support of my aspirations. They are my cornerstone, without whom I could not stand.

NOMENCLATURE

A	Area
A_C	Centrifugal compressor effective area
A_C	Choke area (volume-choke-volume)
A_T	Centrifugal compressor throttle effective area
A_V	Reciprocating compressor valve effective flow area
B	Bulk Modulus
B	Non-dimensional Greitzer model constant
$[B]$	Gradient of the shape function
B_G	Global connectivity matrix
C	Pressure rise across the centrifugal compressor
c_0	Speed of sound
$[C]$	Acoustic damping matrix
$[C_e]$	Acoustic elemental damping matrix
C_{SS}	Steady state centrifugal compressor pressure rise
D	Volume diameter (volume-choke-volume)
d	Choke diameter (volume-choke-volume)
E	Number of elements
F	Pressure drop through the centrifugal compressor throttle
f	Frequency
G	Non-dimensional Greitzer model constant
J	Jacobian matrix
k	Ratio of specific heats
$[K]$	Acoustic stiffness matrix
$[K_e]$	Acoustic elemental stiffness matrix

L	Length
l	Reciprocating compressor rod length
L_C	Centrifugal compressor effective length
L_C	Choke length (volume-choke-volume)
$L_C{}'$	Effective choke length (volume-choke-volume)
L_T	Centrifugal compressor throttle effective length
$\dot{m}$	Mass flow rate
$[M]$	Acoustic mass matric
$[M_e]$	Acoustic elemental mass matrix
$\dot{m}_C$	Centrifugal compressor mass flow rate
$\dot{m}_{OUT}$	Mass flow rate out of the reciprocating compressor cylinder
$\dot{m}_S$	Mass flow rate through surface S
$\dot{m}_T$	Centrifugal compressor mass flow rate
N	Pressure shape function
N	Number of centrifugal compressor rotor revolutions for instability to fully develop
n	Normal vector
N'	Displacement shape function
P	Pressure
P_0	Mean pressure component
$P_{ACOUSTIC}$, P'	Acoustic fluctuation pressure component
P_C	Pressure at centrifugal compressor exit
$P_{C,SS}$	Steady state pressure at centrifugal compressor exit
P_e	Elemental pressure
P_{in}	Pressure at centrifugal compressor suction
P_P	Centrifugal compressor plenum pressure

P_{pipe}	Mean pipe pressure
P_R	Reciprocating compressor cylinder pressure
P_{TOT}	Total pressure
P_V	Pressure at centrifugal compressor plenum
ΔP	Pressure rise in the centrifugal compressor plenum
R	Centrifugal compressor mean rotor radius
r	Reciprocating compressor crank radius
$[R_e]$	Element interface vector
$[R_F]$	Finite element model forcing term
S	Integration surface
S	Reciprocating compressor cylinder area
SM	Surge margin
U	Particle displacement
U	Centrifugal compressor mean rotor velocity
U_e	Elemental displacement
V	Volume
v	Velocity
$\vec{v}'$	Acoustic fluctuation velocity component
v_C	Gas velocity through the centrifugal compressor
v_{IN}	Gas velocity into the reciprocating compressor cylinder
v_{OUT}	Gas velocity out of the reciprocating compressor cylinder
V_P	Centrifugal compressor plenum volume
v_R	Reciprocating compressor piston velocity
v_T	Gas velocity through the centrifugal compressor throttle
x	Reciprocating compressor piston position relative to top dead center

x	Tetrahedral element x global coordinate
Y	Gas compressibility factor
y	Tetrahedral element y global coordinate
z	Tetrahedral element z global coordinate
α	Scalar coefficient for damping
$\alpha_1, \alpha_2, \alpha_3, \alpha_4$	Tetrahedral element shape function coefficient
β	Scalar coefficient for damping
$\beta_1, \beta_2, \beta_3, \beta_4$	Tetrahedral element shape function coefficient
$\gamma_1, \gamma_2, \gamma_3, \gamma_4$	Tetrahedral element shape function coefficient
$\delta_1, \delta_2, \delta_3, \delta_4$	Tetrahedral element shape function coefficient
ζ	Tetrahedral element z local coordinate
ζ	Damping coefficient
η	Tetrahedral element y local coordinate
θ	Angle
ξ	Tetrahedral element x local coordinate
ρ_0 , ρ'	Mean density component
$\rho_{ACOUSTIC}$	Acoustic fluctuation density component
ρ_P	Centrifugal compressor plenum density
ρ_{TOT}	Total density
τ	Time constant
Φ	Orthogonality vector
ω	Rotational velocity
ω	Centrifugal compressor Helmholtz frequency

TABLE OF CONTENTS

Page

LIST OF FIGURES

Page

LIST OF TABLES

Page

1 INTRODUCTION

In natural gas compression systems, reciprocating compressors and centrifugal compressors are often used in combination, particularly at compressor stations used for the long distance transmission of gas. Different types of compressors can be used in both series and parallel arrangements, adding significant operational value to the system. The mixed arrangement seeks to take advantage of the benefits of each type of compressor, namely the flexibility of a centrifugal compressor and the high compression ratio of a reciprocating compressor. However, with these complementary virtues often comes unwanted side effects resulting from increased complexity. Because of the cyclic nature of a reciprocating compressor, they tend to cause periodic pressure pulsations in the gas piping system. The pulsations originate at a frequency equal to the reciprocating compressor's operating speed and its harmonics, and interact with the acoustic properties of the piping system. In the worst case, the pressure pulsations occur at a frequency corresponding to a natural frequency of the pipe system, which significantly amplifies the pulsations. If the amplified pressure pulsations then travel downstream, they can affect other machinery in the piping system, such as a centrifugal compressor. When a centrifugal compressor is exposed to high amplitude pressure fluctuations, the operating point of the centrifugal compressor can be significantly impacted, and can cause the centrifugal compressor to operate at in an unstable region, particularly the high discharge pressure, low flow condition known as surge. In this condition, flow reversal and high vibration can occur, and if the condition persists for a sustained period of time, damage to the machine is likely.

As a result of the desire to operate compressors in a mixed system, it becomes necessary to mitigate the risks associated with the negative aspects of the system interaction (pulsations and surge). This is most commonly done by attenuating the pulsations (using well-developed industry practices such as pulsation dampeners), or by avoiding the unstable region of a centrifugal compressor's operating map. However, attenuation of certain pulsation frequencies does not necessarily inhibit surge, even when surge limits are avoided, due to the interaction between the two. Furthermore, the effects of the interaction on the resulting instability are not well defined in an analytical sense, making numerical simulation a worthy solution. Therefore, it is worthwhile to develop a finite element model of the mixed compressor and piping system, with certain initial

operating conditions, and simulate the response. The simulation will ultimately be packaged in a user-friendly software program, so that pulsations and surge can be predicted and avoided in the design phase.

Reciprocating compressors consist of a piston in a cylinder. The piston is attached to a crankshaft, which rotates to drive the piston back and forth inside the cylinder. When the piston moves in such a way to increase cylinder volume, the pressure inside the cylinder decreases until it is below the supply header pressure. At this point, the differential pressure across the suction valve opens, allowing low pressure gas to enter the cylinder. As the piston reaches the point of highest volume, known as bottom dead center, the piston changes direction and begins to reduce cylinder volume, compressing the gas and raising pressure. The suction valve shuts when cylinder pressure rises above suction header pressure. When cylinder pressure increases above the discharge header pressure, the discharge valve is opened by the differential pressure, allowing the high pressure gas to flow out of the cylinder into the discharge header until the piston reaches the point of lowest volume (top dead center). Here cylinder pressure begins to decrease, the discharge valve shuts, and the process repeats. This cyclic motion and periodic discharge of high pressure gas into the discharge pipe is the source of pressure pulsations. Most reciprocating compressors have multiple cylinders, each with compression chambers on either side of the piston, and run at high speeds. High speeds and high compression ratios result in pulsations with large amplitudes.

Centrifugal compressors work to raise the pressure of gases by accelerating low pressure, low velocity gas with a rotating impellor. The impellor converts shaft work into kinetic energy in the gas. The gas is then decelerated in a diffuser or plenum, resulting in an increase in pressure. All centrifugal compressors have an operating curve, or compressor map, that dictates the pressure rise across the compressor as a function of mass flow through the compressor and compressor speed. The compressor map plots the pressure rise (vertical axis) versus flow rate (horizontal axis), with different curves for different compressor speeds. Most compressor maps have a small section with a negative slope at low flow rate, followed by another small section with positive slope at slightly higher flow rates, and finally a large section with a negative slope at high flow rates. The compressor is operated on the portion of the map at high flow rates with negative slope. At this

operating point, the compressor is self-regulating: as flow rate is reduced, discharge pressure increases, causing flow rate to again increase, restoring to compressor's operating point. However, if flow rate is choked enough to force the compressor's operating point into the portion of the curve with positive slope, a continued drop in flow would then cause a drop in discharge pressure, and enter into one of two unstable operating conditions: stall or surge. The point where the compressor map goes from having a positive slope to a negative slope is called the surge limit. Compressors are normally operated with adequate margin between the operating point and the surge limit (typically a 10% surge margin) to prevent instability.

The instability known as stall is the existence non-uniform variations in flow around the circumference of the compressor (stall cells) that rotate around the axis of the compressor. On the other hand, surge causes large, axial variations in flow. In the case of surge, flow decreases and delivery pressure increases along the operating curve, until the slope of the curve becomes positive. Here the operating point will jump from the characteristic curve to a region of reduced flow where the slope of the characteristic curve is again negative. Then pressure will decrease along the curve and flow will increase until the slope changes sign again, causing the compressor to jump to a region of higher flow and negative slope. Again, flow will begin to reduce and pressure increase until the cycle repeats. The large flow fluctuations that occur during surge can cause large transient forces on the compressor impellors, which can damage bearings and cause rubbing, leading to reduced lifespan or catastrophic failure.

Evidence from the field, as well as research studies, have shown that pressure pulsations in compressor systems exist, and that they can cause high vibrations in attached piping. Pulsations are serious enough that various methods of attenuating them have been devised, with great affect, over the years. Furthermore, anecdotal field evidence suggests that centrifugal compressors have a tendency to go into surge in the presence of high pulsations when they normally would not. However, no studies have coupled pipeline pulsations with centrifugal compressor dynamics in a finite element model. The model developed here bridges that gap by coupling a model of piping system acoustics with a model for compressor surge. Then, a variety of numerical studies are performed to relate compressor surge with pulsation frequency, pulsation

amplitude, and pipe system natural frequency. As a result of this work, engineers designing and operating compressor systems can gain a deeper understanding of how centrifugal compressors react to the existence of pressure pulsations, and can plan to mitigate the risk prior to a potentially damaging situation.

1.1 Literature Review

The basics of acoustic phenomenon are well described in various textbooks. The preferred references here are Kinsler, et al (Kinsler, 2000), and Blackstock (Blackstock, 2000). Fluids obey conservation of mass, conservation of momentum, conservation of energy, and the equations of state, and in fluid acoustics, it is assumed that the fluid is adiabatic and the flow is inviscid. Combining the governing equations results in the linear wave equation. The solution to the wave equation depends on the initial conditions, and the solution is a description of the motion of particles resulting from a perturbation. In piping systems, if the length of a piping span is significantly greater than its diameter, it can be assumed that only a plane wave (flat front, travelling along the length of the pipe) propagates. In the case of plane wave propagation, the wave equation becomes one-dimensional and simple boundary conditions can be applied to determine the natural acoustic frequencies of the pipe. At the open end of a pipe, pressure is zero (pressure release), and at the closed end, velocity is zero. These boundary conditions will result in acoustic natural frequencies that can be calculated algebraically. A cut-off frequency can be calculated as transition point between plane waves and higher order radial and circumferential waves. These types of waves are more likely to occur at a higher excitation frequency, or in large diameter vessels.

Pulsation, in the gas compression industry, generally refers to periodic fluctuations in the local fluid pressure and velocity in a piping system. Wachel and Tison (Wachel, 1994) point out that these fluctuations result most commonly from oscillating flow caused by transmission equipment (particularly reciprocating compressors). They further go on to state that the pulsations are reliant on several factors, including operating conditions, compressor geometry, and thermodynamic relationships, and that the pulsation frequencies occur at quantum values, corresponding to multiples of machine running speed. When the excitation frequency of the system (reciprocating

compressor speed and its multiples) corresponds to an acoustic natural frequency of the attached piping system, the pulsation amplitude is amplified. Furthermore, high amplitude pulsations can couple with the mechanical natural frequency of the piping system, potentially leading to high vibrations. Over the years, the pulsation problem has been corroborated by a steady increase in reciprocating compressor running speed. As a result various methods of controlling and predicting pulsations have been developed.

When pulsations occur in an operating facility, the most common way of controlling them is to attenuate using some type of filter. Wachel and Tison (Wachel, 1994), as well as Damewood (G. Damewood, 1983) describe several types of pulsation filters, with the most common being a volume-choke-volume. The volume-choke-volume acts as a low-pass filter, removing frequency components above its cut-off frequency. The filter is therefore sized such that its cut-off frequency is below the lowest acoustic natural frequency of the downstream piping. The resonant (or Helmholtz) frequency of the filter is calculated algebraically using the dimensions of the system. The cut-off frequency is simply the resonant frequency times the square root of two.

An electro-acoustical analog for modeling piping system acoustics was developed by the Southwest Research Institute in conjunction with the Southern Gas Association as early as the 1950s. As described by Damewood and Nimitz (G. Damewood, Nimitz, W, 1958), the analog approach is enabled by analogous descriptions of pressure, volume displacement, and volume velocity in a fluid system to voltage, charge, and current in an electrical circuit, respectively. As a result, electrical resistance, inductance, and capacitance correspond to acoustical resistance, inertance, and capacitance. Therefore, piping systems and their various components can be accurately simulated by a series of electrical circuits.

The application of finite elements to acoustics problems was first postulated by Gladwell (Gladwell, 1965). The finite element method for acoustics was extended to damped systems by Craggs (Craggs, 1976), and irregular shaped cavities by Petyt, et. al. (Petyt, 1976). Craggs (Craggs, 1985) later states the simple one-dimensional quadratic acoustic mass and stiffness matrices for pipes of varying cross-section, and the constant cross-section case is repeated by Cook (Cook,

2002). Arlett, Bahrani, and Zienkiewicz (Arlett, 1968) further the work by solving the Helmholtz equation in two and three dimensions using finite elements. Kagawa, Yamabuchi, and Mori (Kagawa, 1977), simulate acoustic transmission through various sound tubes using axisymmetric finite elements, with absorption included, and compare the results to experimental data. Bermudez, Hervella-Nieto, and Rodriguez (Bermudez, 1999) assess the interaction between fluids and structures in the transmission of acoustic waves using tetrahedral three-dimensional finite elements. While finite element applications to acoustic problems are in great abundance, those mentioned previously are the primary studies of most use here.

In addition to the studies and analyses performed in the aforementioned articles, a variety of references for the development of an acoustic finite element simulation also exist. Cook (Cook, 2002) is a great reference for general finite element theory, and includes a section dedicated to acoustics. The text describes the finite element formulation of the solution to the wave equation, and derives the mass and stiffness matrices for the one-dimensional case. The ANSYS technical manual (*ANSYS Theory Reference Release 5.6*, 1999) also describes the finite element formulation of the wave equation, the derivation of the fluid matrices, and the derivation of the shape functions for various element shapes. Desmet (Desmet, 2002)provides a detailed description of the finite element formulation of acoustics, including boundary conditions and interfaces. Kattan (Kattan, 2008) has a highly detailed derivation of the stiffness matrix for tetrahedral elements. The procedure outlined is what is used in the calculating the elemental stiffness matrices for use in the finite element computer code. Similarly, Hollauer (Hollauer, 2007) details the procedure for determining the mass matrix for tetrahedral elements. These documents serve as the primary resources for building the acoustic finite element simulation.

An assortment of work in pulsation modelling in gas compressor systems has been done by various researchers in industry and academia, in addition to the electroacoustic analog simulations discussed previously. The study by Tweten, et. al. (Tweten, 2008) includes a computational fluid dynamics (CFD) approach to solving the Navier-Stokes equations for compressible flow in a pipe system, based on the presumption that the assumptions made by the wave equation are too broad for the large amplitude pulsations occurring in gas compression systems. Their comparison of CFD

analysis to the acoustic approach in a 1000 meter long pipe shows that for weak pulsations over any distance from the source, and for strong pulsations at a short distance, the acoustic and fluid dynamic solutions are matched very closely. However, the acoustic solution for large amplitude pulsations which have travelled far from the source begins to diverge from the fluid dynamic solution. The acoustic solution predicts that the pulse continues as a pressure wave, while the fluid dynamics approach predicts that the wave will develop into a shock wave. Cyklis (Cyklis, 2010) gives a general description of the various modern methods of modelling pressure pulsations in pipelines, including one dimensional modeling, frequency domain acoustic modelling, and computational fluid dynamics modelling. Liu, et. al. (Liu, 2012) use an acoustic finite element model to simulate pulsation propagation in gas compressor pipelines, and investigate the effect of using a volume-choke-volume pulsation attenuation mechanism. Brun and Kurz (Brun, 2010) developed a computational fluid dynamics software to model pulsations in compressor system piping, using a reciprocating compressor at one end and a centrifugal compressor at the other. Their model uses a solution of the Navier-Stokes equations to calculate how pulsations interact with piping systems, including when pulsation attenuators are included. The model also includes a centrifugal compressor model as a boundary condition, but simplifies the compressor dynamics down to a polynomial describing the operating curve and the fan law relate pressure pulsations to flow velocity.

Good general descriptions of surge and stall are given by Greitzer (E. M. Greitzer, 1976a) and McMillan (McMillan, 2010). Greitzer (E. M. Greitzer, 1976a) developed a system of non-linear first order differential equations to describe the dynamics of a centrifugal compressor in the mid-1970s. The system he describes consists of the series combination of a compressor, pipe, plenum, and throttle, and applies the continuity equation and conservation of momentum to the system. The result relates various differential pressures and flow rates in the system to the geometry of the system. The system of equations he developed are compared to experimental data to determine the driving factors for surge and stall. His experimental results (E. M. Greitzer, 1976b) show that the propensity for a compressor to go into surge vice stall when it becomes unstable depends on the geometry of the compressor, related in a non-dimensional number he calls *B.*

Moore and Greitzer later expand upon the original theory provided by Greitzer (Moore, 1986), as well as the experimental work (E. M. Greitzer, Moore, F K, 1986). Greitzer's model also used by van Helvoirt and de Jager (van Helvoirt, 2007) in a fluid transmission line model of pipe system dynamics to investigate the effect of pulsations on centrifugal compressor stability. This work, along with Tweten's work (Tweten, 2008), are the only two simulations of a combined centrifugal compressor and piping system available. Yoon, et. al. (Yoon, 2011) included acoustics in Grietzer's model in order to assess the use of an active magnetic bearing to control the vibrations resulting from surge events. The piping acoustics are included in this work to address the piping system acoustical interaction with the centrifugal compressor, in order to counteract the forces on the compressor impellor that result from the piping system pressure fluctuations. Toyama, et. al. (Toyama, 1977) completed an experimental study of surge on a high compression ratio centrifugal compressor, measuring inlet pressure and flow, and diffuser pressures to better understand the mechanisms at work during the onset of surge. Hansen, et. al. (Hansen, 1981) perform an experimental study of an instrumented, small centrifugal compressor in surge, and compare the results to those predicted by Greitzer's model. The comparison shows a satisfactory description of the surge oscillations by Greitzer's model.

1.2 Statement of Thesis

The thesis of this work is that compressor system pipeline pressure pulsations can be modelled using the finite element method for acoustics, and can be used to assess the effect of pulsations on the operating stability of a centrifugal compressor in the system. A computer simulation was developed to perform this analysis, which couples the pipeline acoustic finite element model to a centrifugal compressor dynamic model based on the method developed by Greitzer. The simulation, which can account for variable pipeline geometry and compressor characteristics, develops a transient time-domain solution and has shown that pulsations can reduce the surge margin, and under certain pulsation conditions, a centrifugal compressor will enter surge when it otherwise would not if the system were pulsation-free.

1.3 Objectives and Organization

The objectives of this work are:

1. To develop and validate a model of pipeline pulsations using the finite element method;
2. To couple the finite element model with a centrifugal compressor model;
3. To investigate the effect of pressure pulsations in pipelines on centrifugal compressor operation;
4. To understand the effect of various pressure pulsation characteristics on the operational stability of centrifugal compressors, including the circumstances result in instability.

Section 2 describes the theory behind this work, including acoustics, finite elements, reciprocating compressors, and centrifugal compressors. The specific methodology employed for the various models and numerical experiments is covered in Section 3. The results of the numerical experiments performed are presented in Section 4. Finally, Section 5 summarizes the results of this study, draws conclusions from the results found, and provides recommendations for future work on this subject.

2 BACKGROUND THEORY

2.1 Acoustics

In an acoustic system, fluids obey conservation of mass, conservation of momentum, conservation of energy, and the equations of state. The assumptions made in acoustics are that the fluid system is adiabatic (no heat transfer in or out), the fluid is inviscid (viscosity is set to zero), mean flow is insignificant (much less than the speed of sound), and mean fluid pressure and density are constant. The last assumption requires that total fluid pressure and density are the sum of a mean component and a fluctuation, or acoustic, component, denoted by the prime (') symbol: $P_{TOT} = P_0 + P'$ and $\rho_{TOT} = \rho_0 + \rho'$. Mass conservation, momentum conservation, and equation of state result in:

$$\frac{\partial \rho}{\partial t} + \vec{\nabla} \bullet \left(\rho \vec{v} \right) = 0 \qquad \text{(Conservation of mass)}$$

$$\vec{\nabla} P = -\rho_0 \frac{\partial \vec{v}}{\partial t} \qquad \text{(Conservation of momentum, Euler's equation)}$$

$$c_0 = \sqrt{\frac{B}{\rho}} \qquad \text{(Equation of state)}$$

Here, ρ_0 is the mean density, ρ is the acoustic fluctuation in density, v is acoustic particle velocity, P is acoustic pressure, B is the bulk modulus, and c_0 is the speed of sound. To derive the linearized wave equation, first take the divergence of the continuity equation:

$$\nabla \bullet \left(\vec{\nabla} P = -\rho_0 \frac{\partial^2 \vec{x}}{\partial t^2} \right)$$

$$\nabla^2 P = -\rho_0 \frac{\partial^2}{\partial t^2} \left(\nabla \bullet \vec{x} \right)$$

The insert the equation of state:

$$B = -\frac{P}{dV / V} = -\frac{P}{\nabla \bullet \vec{x}}$$

$$\nabla^2 P = -\rho_0 \frac{\partial^2}{\partial t^2} \left(-\frac{P}{B} \right)$$

This results in the linear wave equation:

$$\nabla^2 P = \frac{1}{c_0{}^2}\frac{\partial^2 P}{\partial t^2}$$

In piping systems, if the length of a piping span is significantly greater than its diameter, it can be assumed that only a plane wave (flat front, travelling along the length of the pipe) propagates. In the case of plane wave propagation, the wave equation becomes one-dimensional and simple boundary conditions can be applied to determine the natural acoustic frequencies of the pipe. At the open end of a pipe, pressure is zero (pressure release), and at the closed end, velocity is zero. These boundary conditions will result in acoustic natural frequencies that can be calculated algebraically. The natural frequencies for pipes with simple boundary conditions are shown in table 1. A cut-off frequency can be calculated as transition point between plane waves and higher order radial and circumferential waves. These types of waves are more likely to occur at a higher excitation frequency, or in large diameter vessels. Figure 1 provides a summary of radial (*p = 0, 1, 2…*) and circumferential (*q = 0, 1, 2…*) mode shapes for a circular cross-section.

Pipe Condition	Natural Frequency, f_i (Hz)	Pressure Mode Shape, Ψ_i
Open-Open 	$\frac{ic_0}{2L}$, *i = 1,2,3…*	$\sin\left(\frac{i\pi x}{L}\right)$
Closed-Closed 	$\frac{ic_0}{2L}$, *i = 1,2,3…*	$\cos\left(\frac{i\pi x}{L}\right)$
Open-Closed 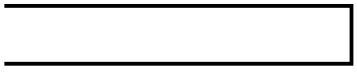	$\frac{(2i-1)\pi}{4L}$, *i = 1,2,3…*	$\sin\left(\frac{(2i-1)\pi x}{2L}\right)$

Table 1. Summary of acoustic natural frequencies and mode shapes for a pipe.

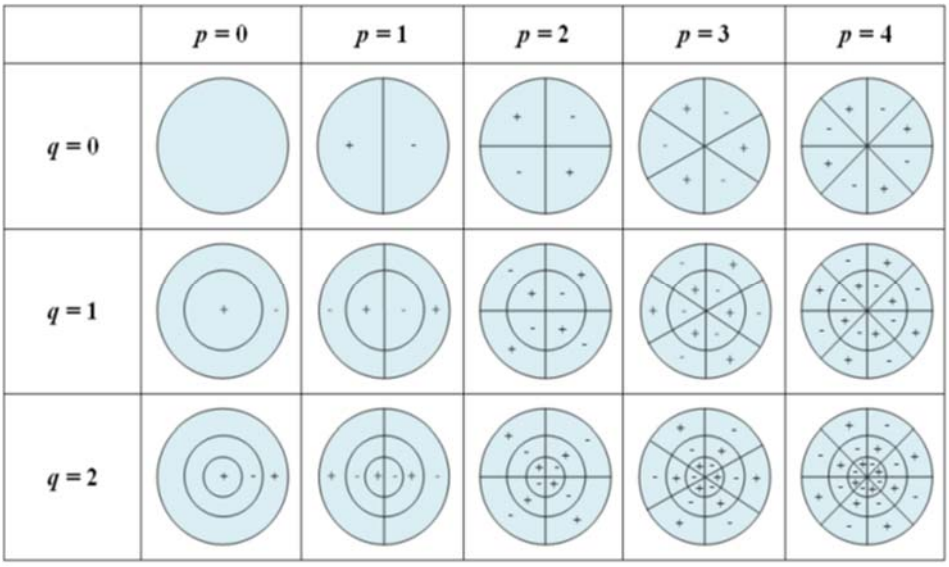

Figure 1. Circumferential and radial acoustic modes of a pipe.

2.2 Pipeline Pulsations and Pulsation Control

As discussed previously, pulsation, in the gas compression industry, generally refers to periodic fluctuations in the local fluid pressure and velocity in a piping system. Pipelines are typically designed with pulsation suppression in mind. A common way of controlling them is by attenuation using some type of filter. The commonly used volume-choke-volume (shown in figure 2), as described by Wachel and Tison (Wachel, 1994) and Damewood (G. Damewood, 1983), functions as a low-pass filter, removing acoustic fluctuations with frequencies above its cut-off frequency. The resonant (or Helmholtz) frequency of the filter is calculated algebraically using the dimensions of the system, as:

$$f = \frac{c}{2\pi}\sqrt{\frac{A_c}{L'_c}\left(\frac{1}{V_1}+\frac{1}{V_2}\right)} \qquad \text{(General volume-choke-volume)}$$

$$f = \frac{c}{\sqrt{2}\pi L}\left(\frac{d}{D}\right) \qquad \text{(Symmetric volume-choke-volume)}$$

For the general case, f is the cut-off frequency (*Hz*), c is the speed of sound (*ft./sec*), A_c is the choke tube cross-sectional area (ft^2), L_c is the choke tube length, $L_c' = L_c + .6d$, d is the choke diameter, and V_1 and V_2 are the volumes of each volume. In a symmetric volume-choke-volume, the volumes

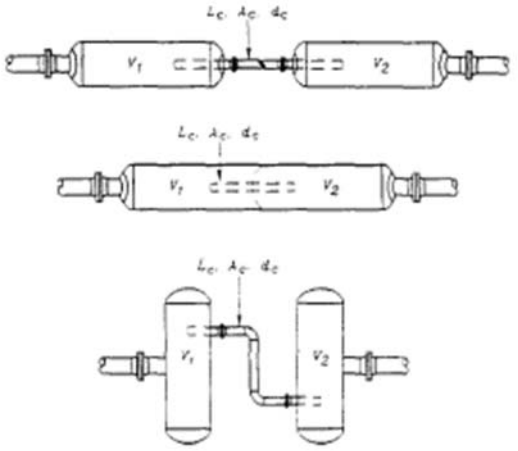

Figure 2. Illustrations of various volume-choke-volume pulsation attenuators.

and choke all have equal length *L*, and the volumes each have equal diameters *D*, which results in the simplified equation. The filter is therefore sized such that its cut-off frequency is below the lowest acoustic natural frequency of the downstream piping. The cut-off frequency is simply the resonant frequency times the square root of two, $f_{co} = 1.414f$.

2.3 Finite Elements

2.3.1 Formulation

Discretization of the wave equation is performed using the Galerkin procedure (Bathe, 1982), outlined in detail in the ANSYS Theory Reference Manual. The wave equation is multiplied by an infinitesimal change in pressure, and integrated over the volume (*ANSYS Theory Reference Release 5.6*, 1999):

$$\int_V \frac{1}{c^2}\delta P \frac{\partial^2 P}{\partial t^2} dV + \int_V \left(\nabla \bullet \delta P\right)\left(\nabla P\right) dV = \int_S \left(n^T \delta P\right)\left(\nabla P\right) dS$$

The surface in the acoustic problem is an interface, and the fluid momentum equation relates to the particle acceleration at the interface by:

$$n\nabla P = -\rho_0 \frac{\partial^2 U}{\partial t^2}$$

Here, *U* is displacement at the interface. Substitution results in:

$$\int_V \frac{1}{c^2}\delta P \frac{\partial^2 P}{\partial t^2} dV + \int_V (\nabla \bullet \delta P)(\nabla P)\, dV = -\int_S \rho_0 \delta P \{n\}^T \frac{\partial^2 \{U\}}{\partial t^2} dS$$

The nodal pressures *P* and displacements *U* are related to the shape functions (*N* for pressure and *N'* for displacement) and elemental pressures P_e and displacements U_e by:

$$P = \{N\}^T \{P_e\}$$

$$U = \{N'\}^T \{U_e\}$$

Therefore, the derivatives of pressure and displacement with respect to time are:

$$\frac{\partial^2 P}{\partial t^2} = \{N\}^T \{\ddot{P}_e\}$$

$$\frac{\partial^2 U}{\partial t^2} = \{N'\}^T \{\ddot{U}_e\}$$

The virtual change in pressure is:

$$\delta P = \{N\}^T \{\delta P_e\}$$

The finite element arrangement of the wave equation therefore becomes:

$$\int_V \frac{1}{c^2} \{\delta P_e\}^T \{N\}\{N\}^T dV \{\ddot{P}_e\} + \int_V \{\delta P_e\}^T [B]^T [B] dV \{P_e\}$$
$$+ \int_S \rho_0 \{\delta P_e\}^T \{N\}\{n\}^T \{N'\}^T dS \{\ddot{U}_e\} = \{0\}$$

Here, *[B]* is the matrix resulting from determining the gradient of each shape function:

$$[B] = \nabla \{N\}^T$$

Dividing by the infinitesimal change in nodal pressure results in:

$$\int_V \frac{1}{c^2} \{N\}\{N\}^T dV \{\ddot{P}_e\} + \int_V [B]^T [B] dV \{P_e\}$$
$$+ \int_S \rho_0 \{N\}\{n\}^T \{N'\}^T dS \{\ddot{U}_e\} = \{0\}$$

Arranging with matrix notation gives the discretized wave equation (equation of motion), the definition of the mass and stiffness matrices, and the definition of the interface vector:

$$[M_e]\{\ddot{P}_e\}+[K_e]\{P_e\}+\rho_0[R_e]\{\ddot{U}_e\}=\{0\}$$

$$[M_e]=\int_V \frac{1}{c^2}\{N\}\{N\}^T\,dV$$

$$[K_e]=\int_V [B]^T[B]dV$$

$$[R_e]=\int_S \{N\}\{n\}^T\{N'\}^T\,dS$$

Damping in the acoustic system represents absorption of sound at the pipe wall. Damping in the model is approximating using a proportional damping scheme, which is expressed as:

$$[C_e]=\alpha[M_e]+\beta[K_e]$$

Here α and β are scalar coefficients, which can be calculated by orthonormalizing the proportional damping equation as shown:

$$\Phi_i^T[C]\Phi_j=\alpha\Phi_i^T[M]\Phi_j+\beta\Phi_i^T[K]\Phi_j=\begin{cases}0, i\neq j\\ \alpha\tilde{M}_j+\beta\tilde{K}_j, i=j\end{cases}$$

$$\tilde{M}_j=\Phi_j^T[M]\Phi_j,$$

$$\tilde{K}_j=\Phi_j^T[\mathrm{K}]\Phi_j=\omega_j^2\tilde{M}_j$$

Therefore,

$$2\varsigma_j\omega_j\tilde{M}_j=\alpha\tilde{M}_j+\beta\omega_j^2\tilde{M}_j \text{, and } \varsigma_j=\frac{\alpha}{2\omega_j}+\frac{\beta\omega_j}{2}$$

The coefficients α and β can be solved for with two assumed damping coefficients ζ_1 and ζ_2, and two known ω values. In the model, the natural frequencies used are the two lowest natural frequencies calculated by the solving the Eigenvalue problem, and the damping coefficients are assumed. Adding the damping term into the equation of motion results in:

$$[M_e]\{\ddot{P}_e\}+[C_e]\{\dot{P}_e\}+[K_e]\{P_e\}+\rho_0[R_e]\{\ddot{U}_e\}=\{0\}$$

Modal analysis is used to determine the natural frequencies of the finite element system. Damping and external forces are neglected, and the equation of motion reduces to:

$$[M]\ddot{\underline{P}} + [K]\underline{P} = 0$$

System pressure is expressed as $p(t) = \underline{P}e^{-i\omega t}$, where $\underline{P}$ is the complex amplitude, which results in:

$$\left([K] - \omega^2[M]\right)\underline{P} = 0$$

The resulting Eigenvalue problem can then be solved for the natural frequencies and mode shapes.

Boundary conditions are imposed on boundary surfaces enclosing the pipe volume, by choosing the appropriate condition (Desmet, 2002). The condition where the pressure is assigned a predetermined value, such as zero at the open end of a pipe, is given by the Dirichlet condition:

$$P = \overline{P}$$

The case where the prescribed pressure is zero is enforced by removing the rows and columns pertaining to that node from the global matrices. At a closed end of the pipe, the pressure exists as a degree of freedom. At a closed boundary, the particle velocity must be zero, therefore, by Euler's equation, the pressure mode shape must have a slope of zero, which is enforced by the Neumann boundary condition:

$$\frac{\partial P}{\partial n} = 0$$

This boundary condition is included in the functional of the finite element formulation. The final boundary condition is the forcing boundary condition, and is included in the interface term (Arlett, 1968). The interface term in the discretized wave equation, $-\rho[R_e]\{U''_e\}$, works out to be the time rate of change of mass flow rate through the surface by unit analysis:

$$\rho_0[R_e]\left\{\ddot{U}_e\right\} = \frac{\partial}{\partial t}\left(\dot{m}_S\right)$$

This term will act as the interface between the reciprocating compressor model, centrifugal compressor model, and pipe acoustic finite element model.

2.3.2 One-Dimensional Acoustic Finite Elements

Both one-dimensional and three-dimensional acoustic finite elements were developed to encompass the scope of the work. The one dimensional model uses a quadratic element (three nodes per element, figure 3), with shape functions:

$$N = \begin{bmatrix} N_1 \\ N_2 \\ N_3 \end{bmatrix} = \begin{bmatrix} \dfrac{(x_2 - x)(x_3 - x)}{(x_2 - x_1)(x_3 - x_1)} \\ \dfrac{(x_1 - x)(x_3 - x)}{(x_1 - x_2)(x_3 - x_2)} \\ \dfrac{(x_2 - x)(x_1 - x)}{(x_2 - x_3)(x_1 - x_3)} \end{bmatrix}$$

If the element has length *L* and x_1 is at *0*, x_2 at *L/2*, and x_3 at *L*, the shape functions reduce to:

$$N = \begin{bmatrix} \dfrac{2}{L^2}\left(\dfrac{L^2}{2} - \dfrac{3}{2}xL + x^2\right) \\ \dfrac{4}{L^2}\left(-xL + x^2\right) \\ \dfrac{2}{L^2}\left(-\dfrac{xL}{2} + x^2\right) \end{bmatrix}$$

The expressions for elemental acoustic mass and stiffness matrices are:

$$[M_e] = \frac{1}{c^2}\int_{Vol} [N][N]^T \, dV$$

$$[K_e] = \int_{Vol} [B]^T [B] dV \text{ , where } [B] = \begin{bmatrix} \dfrac{\partial}{\partial x} \\ \dfrac{\partial}{\partial y} \\ \dfrac{\partial}{\partial z} \end{bmatrix} [N]^T$$

Integrating over the shape functions for the one dimensional case with constant element cross-section, these become:

$$[M_e] = \frac{A}{c^2}\int_0^L [N][N]^T dx = \frac{AL}{30c^2}\begin{bmatrix} 4 & 2 & -1 \\ 2 & 16 & 2 \\ -1 & 2 & 4 \end{bmatrix}$$

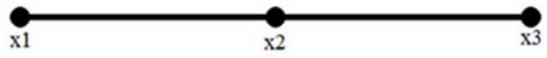

Figure 3. One-dimensional quadratic finite element.

$$[K_e] = A\int_0^L [B]^T [B] dx = \frac{A}{3L}\begin{bmatrix} 7 & -8 & 1 \\ -8 & 16 & -8 \\ 1 & -8 & 7 \end{bmatrix}$$

This result is consistent with work by Craggs (Craggs, 1985), which is summarized by Cook (Cook, 2002). The one dimensional model in this case then only needs the cross-sectional area and length defined for each element to calculate the elemental matrices. The global matrices can be populated using the elemental matrices and a global connectivity matrix (B_G) which is an E by 3 matrix (where E is the number of elements), that specifies the nodes of each element. For a one-dimensional pipe element, the global connectivity matrix is:

$$B_G = \begin{bmatrix} 1 & 2 & 3 \\ 3 & 4 & 5 \\ 5 & 6 & 7 \\ \cdots & \cdots & \cdots \\ 2(E-1)-1 & 2(E-1) & 2(E-1)+1 \\ 2E-1 & 2E & 2E+1 \end{bmatrix}$$

See appendix A for specifics on the one dimensional finite element global matrix assembly procedure.

2.3.3 Three-Dimensional Acoustic Finite Elements

The three dimensional model uses a linear tetrahedral element (figure 4). The same general integral expressions for the acoustic mass and stiffness matrices are used. The element stiffness matrix is determined as follows (Kattan, 2008), where the shape functions for a tetrahedral element are given as:

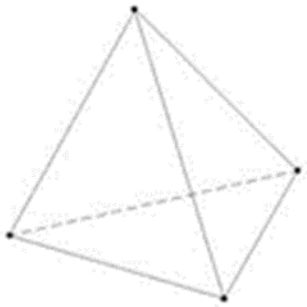

Figure 4. Three-dimensional linear tetrahedral finite element.

$$N_i = \frac{1}{6V}(\alpha_i + \beta_i x + \gamma_i y + \delta_i \, \mathrm{z}) \text{, with } 6V = \begin{vmatrix} 1 & x_1 & y_1 & z_1 \\ 1 & x_2 & y_2 & z_2 \\ 1 & x_3 & y_3 & z_3 \\ 1 & x_4 & y_4 & z_4 \end{vmatrix}$$

Each shape function N_i has its own constants (α_i, β_i, γ_i, and δ_i), and there are four shape functions per element, one for each node. By applying these shape functions to each node in an element so that the equation for the planar face of the element that does not pass through the node equals 1, the coefficients α_i, β_i, γ_i, and δ_i can be determined by Cramer's rule. For example, to calculate α_1, β_1, γ_1, and δ_1 set:

$$\left[N_1\right] = \frac{1}{6V}\begin{bmatrix} 1 & x_1 & y_1 & z_1 \\ 1 & x_2 & y_2 & z_2 \\ 1 & x_3 & y_3 & z_3 \\ 1 & x_4 & y_4 & z_4 \end{bmatrix}\begin{bmatrix} \alpha_1 \\ \beta_1 \\ \gamma_1 \\ \delta_1 \end{bmatrix} = \begin{bmatrix} 1 \\ 0 \\ 0 \\ 0 \end{bmatrix}$$

$$\det\left(\frac{1}{6V}\begin{bmatrix} 1 & x_1 & y_1 & z_1 \\ 1 & x_2 & y_2 & z_2 \\ 1 & x_3 & y_3 & z_3 \\ 1 & x_4 & y_4 & z_4 \end{bmatrix}\right) = \frac{6V}{6V} = 1$$

Therefore:

$$\alpha_1 = \begin{vmatrix} x_2 & y_2 & z_2 \\ x_3 & y_3 & z_3 \\ x_4 & y_4 & z_4 \end{vmatrix}, \beta_1 = -\begin{vmatrix} 1 & y_2 & z_2 \\ 1 & y_3 & z_3 \\ 1 & y_4 & z_4 \end{vmatrix},$$

$$\gamma_1 = \begin{vmatrix} 1 & x_2 & z_2 \\ 1 & x_3 & z_3 \\ 1 & x_4 & z_4 \end{vmatrix}, \delta_1 = -\begin{vmatrix} 1 & x_2 & y_2 \\ 1 & x_3 & y_3 \\ 1 & x_4 & y_4 \end{vmatrix}$$

Repeating this process to find α_i, β_i, γ_i, and δ_i for *i = 2, 3, & 4*, and then solving for *[B]*:

$$[B] = \begin{bmatrix} \frac{\partial}{\partial x} \\ \frac{\partial}{\partial y} \\ \frac{\partial}{\partial z} \end{bmatrix} [N]^T = \frac{1}{6V} \begin{bmatrix} \beta_1 & \beta_2 & \beta_3 & \beta_4 \\ \gamma_1 & \gamma_2 & \gamma_3 & \gamma_4 \\ \delta_1 & \delta_2 & \delta_3 & \delta_4 \end{bmatrix}$$

Thus, the element stiffness matrix can be calculated if the nodal coordinates are known, using the relation:

$$[K_e] = V[B]^T [B]$$

To find the element mass matrix, the following procedure is used (Hollauer, 2007). The element shape functions are transformed from a global coordinate system, *N(x,y,z)*, to a local coordinate system, *N(ξ,η,ζ)*, by the following projection:

$$x = x_1 + (x_2 - x_1)\xi + (x_3 - x_1)\eta + (x_4 - x_1)\zeta$$
$$y = y_1 + (y_2 - y_1)\xi + (y_3 - y_1)\eta + (y_4 - y_1)\zeta$$
$$z = z_1 + (z_2 - z_1)\xi + (z_3 - z_1)\eta + (z_4 - z_1)\zeta$$

The normalized shape functions are then:

$$N_1 = 1 - \xi - \eta - \zeta$$
$$N_2 = \xi$$
$$N_3 = \eta$$
$$N_4 = \zeta$$

The mass matrix integrand becomes:

$$[M_e] = \frac{|J|}{c^2} \int_0^1 \int_0^{1-\xi} \int_0^{1-\xi-\eta} [N(\xi,\eta,\zeta)][N(\xi,\eta,\zeta)]^T \, d\zeta d\eta d\xi$$

Where the Jacobian matrix *[J]* is:

$$[J]=\begin{bmatrix} x_2-x_1 & x_3-x_1 & x_4-x_1 \\ y_2-y_1 & y_3-y_1 & y_4-y_1 \\ z_2-z_1 & z_3-z_1 & z_4-z_1 \end{bmatrix}$$

When the simplified mass matrix integrand is carried out, the mass matrix results in:

$$[M_e]=\frac{|J|}{c^2}\begin{bmatrix} \frac{2}{120} & \frac{1}{120} & \frac{1}{120} & \frac{1}{120} \\ \frac{1}{120} & \frac{2}{120} & \frac{1}{120} & \frac{1}{120} \\ \frac{1}{120} & \frac{1}{120} & \frac{2}{120} & \frac{1}{120} \\ \frac{1}{120} & \frac{1}{120} & \frac{1}{120} & \frac{2}{120} \end{bmatrix}$$

Once again, the element mass matrix can be calculated as long as the nodal coordinates are known. See appendix A for specifics on the three dimensional finite element global matrix assembly procedure.

2.4 Reciprocating Compressor Model

The reciprocating compressor interacts with the piping system by causing a cyclic mass flow into the pipe. To analyze the compressor cylinder, the volume of gas inside the cylinder is chosen as a system, which has three operating conditions: inlet valve only open, discharge valve only open, and both valves shut. With both valves shut, conservation of mass requires:

$$\dot{m}=\frac{d\rho V}{dt}=\frac{d}{dt}\left(x\rho S\right)=\rho S\frac{dx}{dt}+xS\frac{d\rho}{dt}=0$$

Here, *x* is the position of the compressor cylinder relative to top dead center (in the direction of stroke), *ρ* is the gas density, and *S* is the cylinder face area. Treating gas in the compressor cylinder as a polytropic process requires:

$$\frac{P}{\rho^k}=const.=\frac{P_0}{{\rho_0}^k}$$

Combining the polytropic relation with the conservation of mass results in the following expression, where the subscript *R* refers to the reciprocating compressor cylinder, and v_R is the

velocity of the piston:

$$\frac{\partial P_R}{\partial t} = -\frac{v_R}{xk} P_R$$

With the discharge valve open the system is open, allowing mass flow through the valve. Conservation of mass becomes:

$$\dot{m} = \frac{d}{dt}\left(x\rho S\right) = \rho S \frac{dx}{dt} + xS\frac{d\rho}{dt} = -\dot{m}_{OUT} = -\rho v_{OUT} A_V$$

Here, the mass flow rate is through the discharge valve, v is the gas velocity in the valve, and A_V is the valve flow area. The density is assumed to be equal to the density in the cylinder and constant through the valve. Applying the polytropic process relation results in:

$$\frac{\partial P_R}{\partial t} = -\frac{P_R}{xSk}\left(-Sv_R - v_{OUT} A_V\right)$$

Similarly, conservation of mass when the suction valve is open is:

$$\dot{m} = \frac{d}{dt}\left(x\rho S\right) = \rho S \frac{dx}{dt} + xS\frac{d\rho}{dt} = \dot{m}_{IN} = \rho v_{IN} A_V$$

The sign of the mass flow rate term is now positive due to flow being in the opposite direction. The differential equation for pressure becomes:

$$\frac{\partial P_R}{\partial t} = -\frac{P_R}{xSk}\left(-Sv_R + v_{IN} A_V\right)$$

Combining the mass conservation equations results in the conditional differential equation that governs pressure inside the reciprocating compressor cylinder:

$$\frac{\partial P_R}{\partial t} = \begin{cases} -\dfrac{P_R}{xSk}\left(-Sv_R - v_{OUT} A_V\right) & P_R < P_{OUT} \\ -\dfrac{P_R}{xSk}\left(-Sv_R + v_{IN} A_V\right) & P_R < P_{IN} \\ -\dfrac{v_R}{xk} P_R & else \end{cases}$$

To determine cylinder position, a simple linkage mechanism (figure 5) is analyzed. Using a vector analysis to specify position:

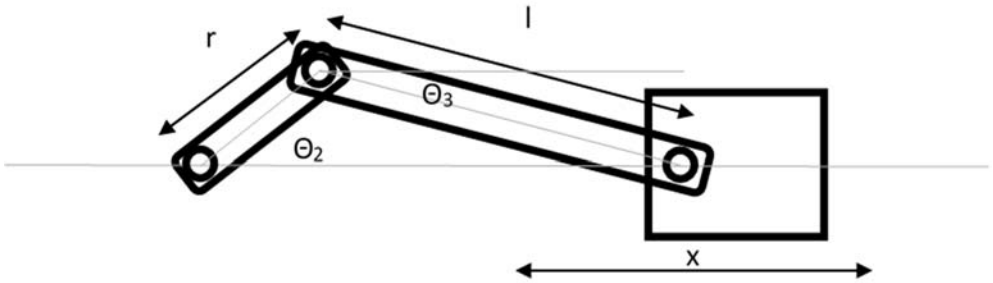

Figure 5. Piston-cylinder mechanism.

$$-xe^{j\theta_1} + re^{j\theta_2} - le^{j\theta_3} = 0$$

Here, *x* is the position of the piston, Θ_1 is the piston angle, *r* is the crank length, Θ_2 is the crank angle, *l* is the rod length, and Θ_3 is the rod angle. Writing the real and imaginary parts, and setting Θ_1 equal to zero results in:

$$x = l\cos\theta_3 - r\cos\theta_2$$
$$0 = -l\sin\theta_3 + r\sin\theta_2$$

The crank angle Θ_2 is equal to the product of angular velocity and time. Rearranging to eliminate Θ_3 results in the piston position equation:

$$x(t) = l\cos\left(\sin^{-1}\left(\frac{r}{l}\sin(\omega t)\right)\right) - r\cos(\omega t)$$

The piston position and velocity are inserted into the equation for cylinder pressure, as described above.

The velocity through the valve is derived from the Bernoulli equation, and is the commonly known flow equation:

$$v = Y\sqrt{\frac{2}{\rho}\Delta P}$$

The flow equation is applicable for incompressible flows, and approximates the flow through a valve by a compressible gas if the compressibility factor *Y* is introduced. A typical value for *Y* is *.6* to *.7*. The density used in the equation is the upstream density.

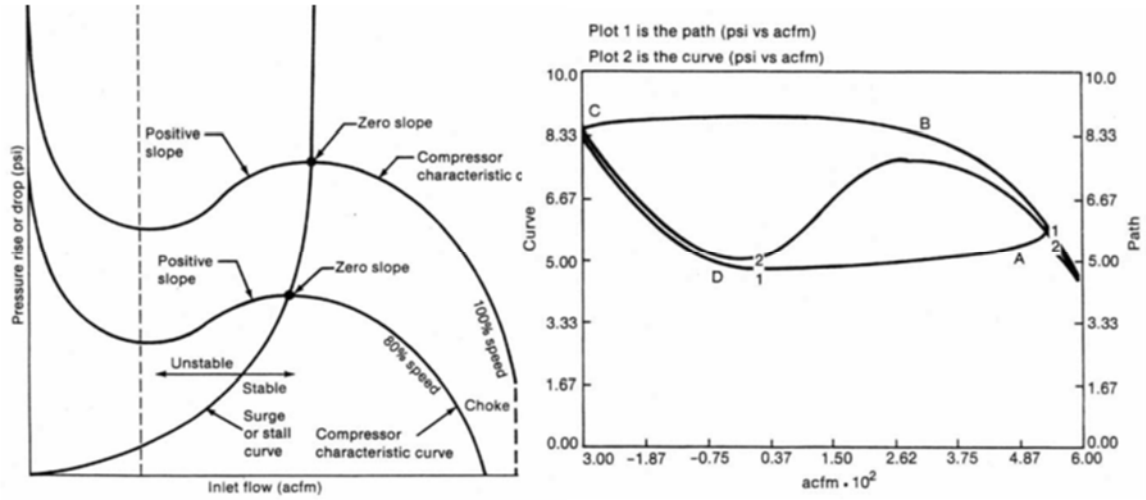

Figure 6. (a) Compressor map (left). (b) Surge path (right).

2.5 Centrifugal Compressor Model

The operation of a centrifugal compressor is dictated by its compressor map, which is a plot of compressor flow versus pressure rise (figure 6a). The operating curve shows what the compressor rise across the compressor will be for a given flow and speed. The curve typically has a negatively sloped section at low flow, a positively sloped section at higher flow, and a negatively sloped section at the operating flow rates. The point on the curve where the slope goes from positive to negative is referred to as the surge limit. A curve connecting the surge limit points of all the speed curves is called the surge curve. When a compressor operates on the negatively sloped portion of the curve, the compressor is self-regulating because a drop in flow rate (from the partial shutting of a downstream throttle valve, for example) will cause the pressure rise to increase, and the flow rate to resultantly increase, hence restoring the compressor's operating point. When the operating point crosses the surge limit however, the compressor will become unstable, and potentially follow a surge cycle, shown in figure 6b. This cycle results in large fluctuations in pressure and flow within the compressor, which can result in machine damage.

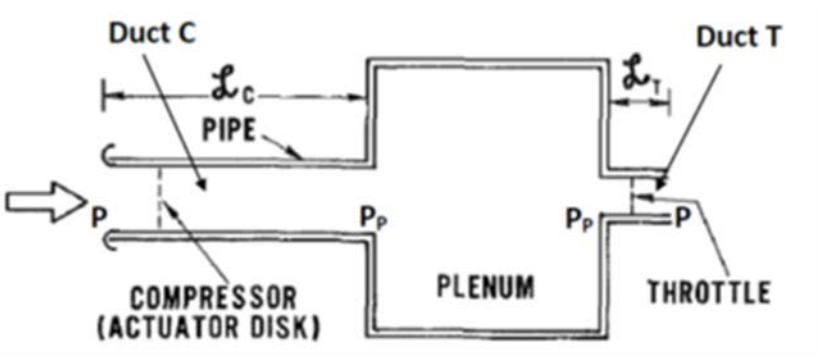

Figure 7. Equivalent compressor system used in Greitzer's analysis (E. M. Greitzer, 1976a).

Greitzer (E. M. Greitzer, 1976a) developed a model for the dynamic operation of a general centrifugal compressor, which consists of a compressor, pipe, plenum, and throttle using figure 7. Applying the inviscid, one dimensional momentum equation with constant velocity across the compressor duct results in the relation for the change in mass flow rate through the compressor duct:

$$\frac{dv_C}{dt} = -\frac{1}{\rho}\frac{dp}{dx}$$

$$\frac{dv_C}{dt} = -\frac{1}{\rho}\frac{(\Delta P - C)}{L_C}$$

$$\frac{d\dot{m}_C}{dt} = \frac{A_C}{L_C}(C - \Delta P)$$

Here, C is the pressure rise across the duct, ΔP is the pressure rise at the plenum, A_C is the effective compressor area, and L_C is the effective compressor length. The change in mass flow through the throttle duct is found in a similar fashion:

$$\frac{dv_T}{dt} = -\frac{1}{\rho}\frac{dp}{dx}$$

$$\frac{dv_T}{dt} = -\frac{1}{\rho}\frac{(F - \Delta P)}{L_T}$$

$$\frac{d\dot{m}_T}{dt} = \frac{A_T}{L_T}(\Delta P - F)$$

Again, F is the pressure drop across the throttle, A_T is the effective throttle area, and L_T is the effective throttle length. The throttle pressure drop is related to the velocity through the throttle by the Bernoulli equation:

$$F = \frac{1}{2}\rho v_T^2 = \frac{\dot{m}_T^2}{2\rho A_T^2}$$

Assuming that the velocity in the plenum is negligible, the continuity equation can be applied to the plenum:

$$\frac{\partial \rho}{\partial t} + \nabla \bullet (\rho v) = 0$$

$$\frac{d\rho}{dt} + \rho \frac{dv}{dt} = 0$$

$$\frac{d\rho}{dt} = \frac{\rho}{\Delta x}(v_C - v_T) = V_P(\dot{m}_C - \dot{m}_T)$$

Here, V_P is the plenum volume. The process in the plenum can be assumed polytropic. Hence:

$$\frac{P}{\rho^k} = const. = \frac{P_0}{\rho_0^k}$$

$$\frac{d\rho}{dt} = \frac{\rho}{kP}\frac{dP}{dt}$$

Inserting into the continuity equation results in:

$$\frac{dP_P}{dt} = \frac{kP_P}{\rho_P} V_P(\dot{m}_C - \dot{m}_T)$$

Here, P_P is the pressure in the plenum, ρ_P is the density in the plenum, and k is the polytropic exponent, which can be assumed to be equal to the ratio of specific heats for the gas in the system.

The final unknown in the system is the compressor pressure rise C. In a real system, there is a time lag on the order of about eight rotor revolutions between the onset of an instability and its full development. Greitzer choses to model this lag as a first order transient response in compressor pressure rise relative to the steady-state compressor rise read from the compressor map C_{SS}. The explicit response with time constant τ is:

$$\frac{dC}{dt} = \frac{1}{\tau}\left(C_{SS} - C\right)$$

The time constant is calculated from:

$$\tau = \frac{2\pi RN}{U}$$

Where *R* is the mean rotor radius, *N* is the approximate number of rotor revolutions to reach a fully developed state of instability, and *U* is the mean rotor velocity.

Greitzer then non-dimensionalizes his equations by dividing the mass flows by the mass flow through the compressor $\rho U A_C$, the pressures by a representative pressure $\frac{1}{2}\rho U^2$, and time by a characteristic time $1/\omega$, where ω is the Helmholtz frequency of the equivalent compressor duct with speed of sound *c*:

$$\omega = c\sqrt{\frac{A_C}{V_P L_C}}$$

The resulting set of equations is:

$$\frac{d\dot{\tilde{m}}_C}{d\tilde{t}} = B\left(\tilde{C} - \Delta\tilde{P}\right)$$

$$\frac{d\dot{\tilde{m}}_T}{d\tilde{t}} = \frac{B}{G}\left(\Delta\tilde{P} - \tilde{F}\right)$$

$$\frac{d\Delta\tilde{P}}{d\tilde{t}} = \frac{1}{B}\left(\dot{\tilde{m}}_C - \dot{\tilde{m}}_T\right)$$

$$\frac{d\tilde{C}}{d\tilde{t}} = \frac{1}{\tilde{\tau}}\left(\tilde{C}_{SS} - \tilde{C}\right)$$

The tilde (~) over the variables indicates that they have been non-dimensionalized. The above equations also introduce two new non-dimensional parameters, *B* and *G*, defined as:

$$B = \frac{U}{2\omega L_C} = \frac{U}{2c}\sqrt{\frac{V_P}{A_C L_C}}$$

$$G = \frac{L_T A_C}{L_C A_T}$$

The non-dimensional time constant is:

$$\tilde{\tau} = \frac{2\pi NR\omega}{U} = \frac{\pi NR}{L_C B}$$

The non-dimensional pressure drop through the throttle is:

$$\tilde{F} = \frac{v_T^2}{U^2} = \frac{\dot{m}_T^2}{\rho^2 U^2 A_T^2} = \frac{A_C^2 \tilde{\dot{m}}_T^2}{A_T^2}$$

Greitzer numerically develops transient solutions to this set equations for compressors with *B* values of *.45*, *.60*, *.70*, *1.58*, and *5.00*. His results indicate that a compressor with a *B* value of *.7* or greater will tend toward surge when their surge limit is reached. Compressors with lower *B* values will tend toward a different type of instability, known as stall. Greitzer then applies his model to an experimental test compressor with variable speed and a variable plenum volume, allowing for the variation of *B*. His experimental results (E. M. Greitzer, 1976b) compare well to his numerical results, and confirm his hypothesis that surge will occur above a *B* value of about *.7*, and stall will occur below it. Changes in *G* tend to have a negligible effect on the systems tendency toward surge or stall.

The proximity of a centrifugal compressor's operating point to the surge limit is quantified by the surge margin, which is related the mass flow rate where the surge limit line intersects the operating curve for a given speed. The surge margin *SM* is defined as (Kurz, 2004):

$$SM = 100\% \times \left(\frac{\dot{m}_c - \dot{m}_{surge}}{\dot{m}_c} \right)\Bigg|_{speed=const.}$$

It is common to maintain a surge margin of approximately ten percent or more for an operating centrifugal compressor.

3 METHODOLOGY

To approach the problem of analyzing a compressor and piping system model, a model of the piping system response was developed using an acoustic finite element method, as outlined in the theory section. This model must be robust enough to handle complex piping geometries as well as steady-state and transient response. The transient response will be necessary for the dynamic system model. Next, the reciprocating compressor model is coupled to the piping system as a boundary condition. Similarly, a centrifugal compressor model, based on Greitzer's model, is coupled as a boundary condition to the pipe acoustic model at the opposite end of the pipe. The acoustic finite element model is designed to model perturbations around a mean pressure. The full model accounts for this by assuming the pipe mean pressure is constant throughout. Once the system model is fully developed, numerical experimentation is be carried out with a variety of reciprocating compressor geometries, to correspond to a variety of pulsation frequencies and amplitudes. The experiments will show the response of the piping system and the downstream pulsation characteristics. The goal is to see how the reciprocating compressor pulsations affect the centrifugal compressor's proximity to the surge limit. This type of experimental analysis will be useful in aiding industry entities understand how compressor systems will interact with piping system acoustics, and how the margin to surge can be reduced as a result.

3.1 Acoustic Model

One-dimensional and three-dimensional finite element acoustics models for a piping system were developed based on the formulation described in the theory section, and implemented in purpose-built MATLAB codes. The one dimensional model requires the length and cross-sectional area of each element to be defined. Using this information, the code can develop the required coordinates and connectivity matrices. The element lengths and cross-sectional areas are used in determining the elemental mass and stiffness matrices, which are used with the coordinates and connectivity matrices are used to assemble the global mass and stiffness matrices. The three-dimensional model on the other hand requires externally created coordinates and connectivity matrices. For the analysis here, the acoustic space is modelled in SolidWorks, which generates the finite element meshes, and outputs the coordinates and connectivity matrices into a text file. The

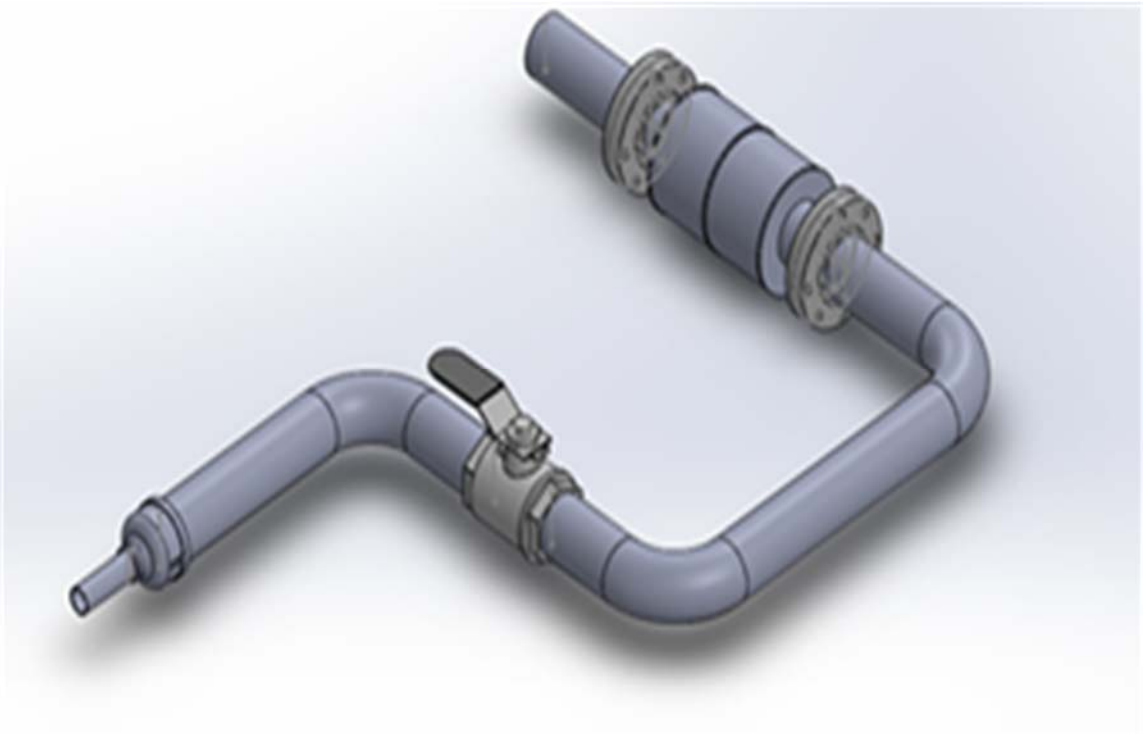

Figure 8. Proof of concept piping system design.

MATLAB code reads the text file and extracts the matrices, rebuilding them in matrix form using MATLAB syntax. Again the coordinates and connectivity matrices are used in calculating the elemental mass and stiffness matrices, which are used to assemble the global mass and stiffness matrices.

To assess the accuracy and capability of the one-dimensional and three-dimensional acoustic finite element models, a small piping system was built. Modal analysis was employed to calculate the natural frequencies and mode shapes of the piping system with the one-dimensional and three-dimensional finite element codes. Then the acoustic response of the system was measured experimentally for comparison to the calculated natural frequencies. In order to determine the ability of the finite element code to handle various changes in pipe geometry, including elbows, reducers, valves, and volume-choke-volumes, the piping model needed to contain all these various elements. Therefore, the piping system in figure 8 was devised. The majority of the pipe is *4* inch schedule 40. It includes a flanged volume-choke-volume, which can be removed and replaced with

Figure 9. Completed proof of concept piping system.

a straight run of *4* inch schedule 40 pipe, three elbows, a 4 inch ball valve, and a reducer to a *1.5* inch outlet section. The completed pipe system is shown in figure 9.

A block diagram of the experimental setup is shown in Figure 10. A white noise generator driving a speaker was used as the excitation source. Two microphones are used for data collection, one at the speaker end for reference and the other at the outlet end. A pre-amplifier provides *+48V* ghost voltage to the microphones. The pre-amplifier output can either be to an oscilloscope, or to a computer via a stereo cable. For this experiment, a personal computer was used for data collection. The pre-amplified passes the analog sound pressure level data from the microphones separately over the left and right channel of the stereo cable. Ten six second sound cuts were taken using the sound recorder included in the Windows 7 operating system. The data from the sound recorder holds the data in a two column array, where each column is either left or right channel sound pressure amplitude. The sound data is then passed to MATLAB for processing, where a fast Fourier transform is performed on each data cut. Then the Fourier transforms are

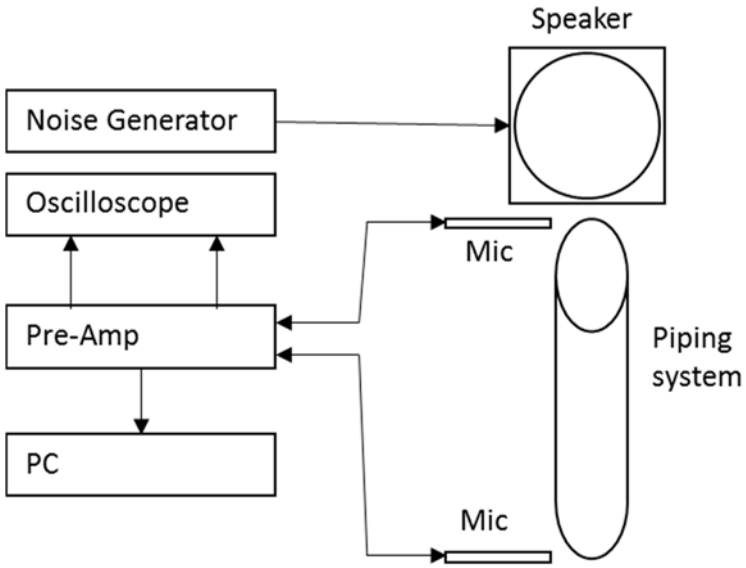

Figure 10. Proof of concept experimental setup.

ensemble averaged to reduce noise. The frequency domain results were then compared to the one dimensional and three dimensional predicted frequency response.

3.2 Reciprocating Compressor Model

The reciprocating compressor interacts with the piping model at the point where the compressor's valves inject high pressure gas into the model. The dynamics of the compressor gas and valve flow are treated previously. The differential equation model is solved for compressor cylinder pressure *P* numerically using MATLAB ODE45. The piston position and velocity are determined algebraically at each time step (assuming constant speed), and the suction and discharge valve conditions are determined by comparing cylinder pressure with suction header pressure and discharge header pressure respectively. The valves in a reciprocating compressor open and shut based on the differential pressure across them. This is accomplished in the solver by determining the valve area as a function of the differential pressure across the valve. The valve area therefore varies linearly as differential pressure approaches the differential pressure required for maximum valve lift. An

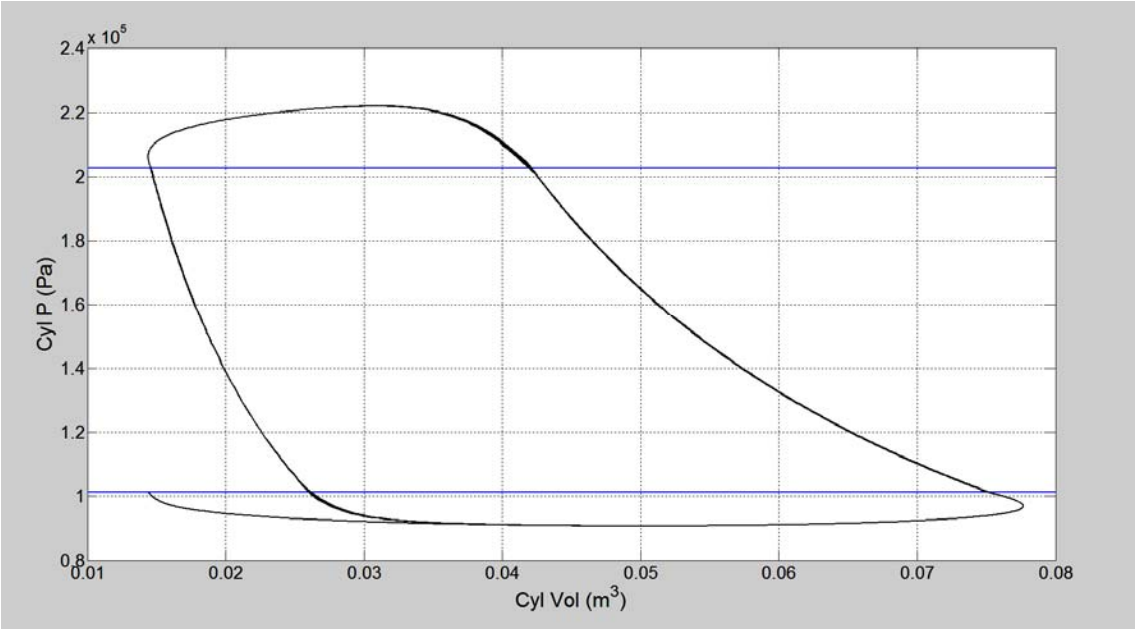

Figure 11. Solution to reciprocating compressor model.

example of the solution for constant suction and discharge header pressures is shown in figure 11.

3.3 Centrifugal Compressor Model

The centrifugal compressor model outlined previously can be solved quickly and efficiently using the ODE45 function in MATLAB. To do so, parameters from Grietzer's papers (E. M. Greitzer, 1976a) were used, including the compressor operating curve, which can be recreated using a series of points and linear interpolation between the points. The system will converge to a steady state point when the differentials all equal zero, requiring:

$$P_C = P_V = P_{C,SS}$$

$$\dot{m}_C = \dot{m}_T$$

$$P_V - P_{in} = F = \frac{\dot{m}_T^2}{2\rho A_T^2}$$

The throttle curve is created by plotting the pressure drop across the valve *F* against the mass flow

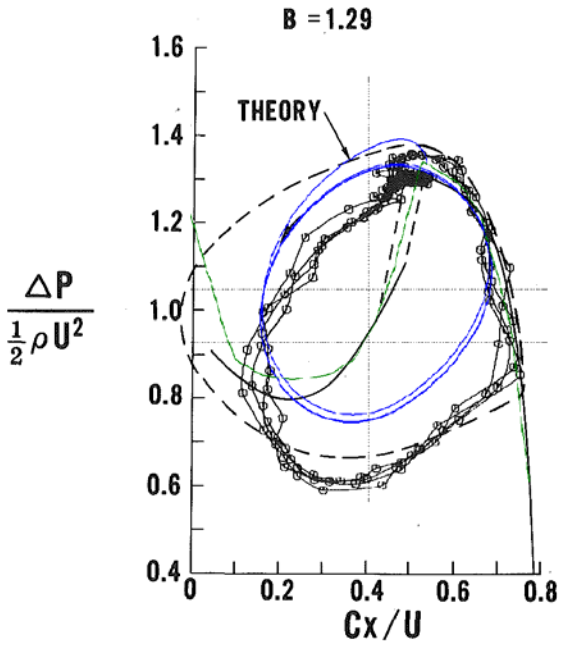

Figure 12. Comparison with Grietzer's solution (E. M. Greitzer, 1976b).

rate through the valve. The mass flow rate is a function of the velocity and throttle area, which in practice is the throttle valve setting. The intersection of this curve with the compressor map is the point at which the steady state conditions are met. The throttle curve is varied by choosing A_T. Therefore, to choose the conditions for the simulation, a desired mass flow and pressure rise are chosen and A_T is calculated by setting F equal to the desired pressure rise. Hence, if the initial conditions meet all the steady state conditions, the system will remain at its initial state during the simulation. If A_T is varied slightly from the initial state to create a small perturbation, the simulation will quickly converge to the new operating point defined by A_T. However, if A_T is perturbed further, with F being driven below the surge limit, the system will become unstable and enter the surge limit cycle.

In Greitzer's numerical experiments, the initial set points for mass flow and pressure were chosen according to a point on the compressor map, and A_T was chosen as the such that the F curve intersects the compressor map beyond the surge limit. In the simulations here, the initial conditions are similarly chosen for a stable operating point, but A_T is chosen for an unstable point,

therefore driving the system into surge. A comparison between Grietzer's results and the MATLAB solution is shown in figure 12 (E. M. Greitzer, 1976b). The MATLAB solution is shown with a solid blue line, and mimic the limit cycle observed by Grietzer's equations (dashed line), and experimental results (open circles with lines).

3.4 Combined Model

To combine the differential equation model of the cylinder model requires adding a load force to the first element of the pipe section, representing the cylinder discharge. The load force acting at the interface, as previously stated, is:

$$\left[R_F\right] = \rho \sum \int \left[N_F\right]^T \ddot{u}_n dS = \rho \ddot{u}_n S = \frac{d\dot{m}}{dt}$$

The mass flow rate through the valve is:

$$\dot{m} = A_v Y \sqrt{2\rho \Delta P}$$

Therefore, the forcing term at the boundary is set equal to the time derivative of the mass flow rate through the valve at any given instant in time.

To include the centrifugal compressor in the model, it is necessary to restore dimension to Greitzer's equations. This is done in the opposite fashion as before, and results in:

$$\begin{bmatrix} \frac{dC}{dt} \\ \frac{d\Delta P}{dt} \\ \frac{d\dot{m}_C}{dt} \\ \frac{d\dot{m}_T}{dt} \end{bmatrix} = \begin{bmatrix} \frac{1}{\tau}\left(C_{SS} - C\right) \\ \frac{c^2}{V_P}\left(\dot{m}_C - \dot{m}_T\right) \\ \frac{A_C}{L_C}\left(C - \Delta P\right) \\ \frac{A_T}{L_T}\left(\Delta P - F\right) \end{bmatrix}$$

The pressure differences can also be removed by expressing them in terms of their components:

$$C = P_C - P_{in}$$
$$C_{SS} = P_{C,SS} - P_{in}$$
$$\Delta P = P_V - P_{in}$$

Here, P_{in} is the compressor suction pressure, P_C is the compressor discharge pressure, $P_{C,SS}$ is the steady-state compressor discharge pressure, and P_V is the plenum pressure. Inserting these into the Greitzer equations gives:

$$\begin{bmatrix} \frac{dP_C}{dt} \\ \frac{dP_V}{dt} \\ \frac{d\dot{m}_C}{dt} \\ \frac{d\dot{m}_T}{dt} \end{bmatrix} = \begin{bmatrix} \frac{1}{\tau}\left(P_{C,SS} - P_V\right) + \frac{dP_{in}}{dt} \\ \frac{c^2}{V_P}\left(\dot{m}_C - \dot{m}_T\right) + \frac{dP_{in}}{dt} \\ \frac{A_C}{L_C}\left(P_C - P_V\right) \\ \frac{A_T}{L_T}\left(P_V - P_{in} - F\right) \end{bmatrix}$$

The centrifugal compressor and piping system are coupled in a manner similar to the coupling between the reciprocating compressor and the piping system. Again, the load force boundary condition must be enforced at the centrifugal compressor end and is equal to the time rate of change of the mass flow rate. Now, however, the mass flow rate through the centrifugal compressor is one of the variables in Grietzer's equations, and its derivative is given by Grietzer's equation:

$$\left[R_F\right] = -\frac{\partial \dot{m}_C}{\partial t} = -\frac{A_C}{L_C}\left(P_C - P_V\right)$$

The negative sign is used here because the centrifugal compressor acts to pull gas out of the pipe.

The finite element formulation is an ordinary second order differential equation of the form:

$$\left[M\right]\left\{\ddot{P}\right\} + \left[C\right]\left\{\dot{P}\right\} + \left[K\right]\left\{P\right\} + \left\{R_F\right\} = \left\{0\right\}$$

To develop a solution using MATLAB's ODE45, the equation must be reduced to a first order differential equation, and rearranged. The reduction is completed by setting:

$$\begin{bmatrix} \underline{P}_1 \\ \underline{P}_2 \end{bmatrix} = \begin{bmatrix} \underline{P} \\ \underline{\dot{P}} \end{bmatrix}$$

Where $\underline{P}$ is a vector of element pressures, which has length equal to the number of nodes N in the model. Therefore, the finite element formulation can be rewritten as:

$$\begin{bmatrix} \dot{\underline{P}}_1 \\ \dot{\underline{P}}_2 \end{bmatrix} = \begin{bmatrix} \dot{\underline{P}} \\ \ddot{\underline{P}} \end{bmatrix} = \begin{bmatrix} \underline{P}_2 \\ [M]^{-1}\left([R_F] - [C]\underline{P}_2 - [K]\underline{P}_1\right) \end{bmatrix}$$

The number of equations required for developing the transient solution to the finite element problem is thus twice the number of degrees of freedom. Adding the reciprocating and centrifugal compressors into the model requires adding one conditional differential equation for each reciprocating compressor cylinder, and four differential equations for the centrifugal compressor. The resulting system of equations is:

$$\begin{bmatrix} \dot{P}_1 \\ \cdots \\ \dot{P}_{1,\mathrm{N}} \\ \dot{P}_{2,i} \\ \cdots \\ \dot{P}_{2,\mathrm{N}} \\ \dot{P}_R \\ \dfrac{\partial P_C}{\partial t} \\ \dfrac{\partial P_V}{\partial t} \\ \dfrac{\partial \dot{m}_C}{\partial t} \\ \dfrac{\partial \dot{m}_T}{\partial t} \end{bmatrix} = \begin{bmatrix} P_{2,i} \\ \cdots \\ P_{2,\mathrm{N}} \\ [M_i]^{-1}\left([R_{F,\mathrm{i}}] - [C_i]P_{2,i} - [K_i]P_{1,i}\right) \\ \cdots \\ [M_N]^{-1}\left([R_{F,\mathrm{N}}] - [C_N]P_{2,\mathrm{N}} - [K_N]P_{1,\mathrm{N}}\right) \\ f(P_R, P_{1,i}, t) \\ \dfrac{1}{\tau}\left(P_{C,SS} - P_V\right) + P_{2,j} \\ \dfrac{c^2}{V_P}\left(\dot{m}_C - \dot{m}_T\right) + P_{2,j} \\ \dfrac{A_C}{L_C}\left(P_C - P_V\right) \\ \dfrac{A_T}{L_T}\left(P_V - P_{pipe} - P_{1,j} - F\right) \end{bmatrix}$$

The centrifugal compressor equations have been modified by replacing the suction pressure P_{in} with the sum of the pipe mean pressure P_{pipe} and the acoustic pressure at node j, P_j, the node connected to the centrifugal compressor. Therefore, the pressure at this node is represented in the system of equations by $P_{1,j}$, and its time derivative is represented by $P_{2,j}$. The pipe mean pressure is constant, so its time derivate is zero.

3.5 Numerical Experimentation Method

The parameter study includes a sinusoidal representation of a reciprocating compressor with

speed f varied from 5 to $200\ Hz$, and amplitude R_0 varied from 5 to $200\ kg/s/s$. The pipe in the study has a length of $2\ m$ and a diameter of $.2\ m$. The reciprocating compressor is replaced with a sinusoidal forcing signal to alleviate some numerical instability resulting from discontinuity due to the reciprocating compressor model, reduce the computation time needed for the experiments, and remove the need to change other system parameters. The interface between the reciprocating compressor and piping acoustics occurs and the reciprocating compressor discharge valve, and the forcing term in the finite element model is the time rate of change of mass flow rate. In a reciprocating compressor, the valves open extremely quickly, and result in a sudden change in mass flow rate, and therefore a nearly discontinuous time rate of change of mass flow rate. This sharp change causes numerical stability problems as the MATLAB ODE solver attempts to converge on a solution near the discontinuity. The result is very slow computation times, on the order of several hours for one second of solution. This makes completing a parameter study nearly impossible.

Secondly, in order to conserve mass in a compressible fluid flow system, the mean pipe pressure must be dependent on the net mass flow (into the pipe from the reciprocating compressor discharge, and out of the pipe to the centrifugal compressor suction), which requires adding a static pipe pressure equation to the simulation. This is possible when a desired reciprocating compressor flow is selected. However, when reciprocating compressor speed is varied, the mass flow rate out of the reciprocating compressor changes, causing an imbalance of flow through the pipe, which results in a dramatic increase or decrease in mean pipe pressure. To counteract this, the reciprocating compressor needs to be resized to match flow rates, which has an effect on pressure pulsation magnitude and makes analyzing the acoustic response much more complicated. Therefore, to simplify the computation and focus on the effect of acoustic fluctuations in pipe pressure on compressor operating point, the mean pipe pressure is maintained constant and a small pressure perturbation is applied as the forcing term.

Therefore, because these experiments are most concerned with the fluctuating portion of the input, the reciprocating compressor is approximated by a sinusoidal input, which will excite the piping system acoustics sufficiently enough to cause oscillation in the centrifugal compressor

operating point. As a result, for the parameter study, the reciprocating compressor is approximated by a sinusoidal input:

$$R_F = R_0 \cos(2\pi ft)$$

The forcing term therefore represents the time rate of change of mass flow rate out of the reciprocating compressor, have units of mass per second squared. For this part of the analysis the centrifugal compressor will be operating at steady state, with the initial flow condition chosen to be firmly in the stable region, and the throttle setting (flow area) is calculated from:

$$A_T = \frac{\dot{m}_C}{\sqrt{2\rho C}}$$

The dimensions of the centrifugal compressor are the same as in Greitzer's analysis, summarized in table 2.

Finally, another series of numerical experiments were carried out with the initial centrifugal compressor operating at a *0.5%* surge margin. The simulation was run over a variety of input fluctuation amplitudes with frequency held constant, and again over a variety of input fluctuation frequencies with amplitude held constant. Each simulation was analyzed for surge, and the average surge margin over the duration of the study was calculated. It is expected that pulsations of sufficient strength will drive the centrifugal compressor into surge, and this series of experiments will aide in predicting such a phenomenon.

Parameter	Value	Parameter	Value
A_C Compressor Area	.1445 m^2	L_C Compressor Length	1.8 m
L_T Throttle Length	.02 m	N Compressor turns for instability to fully develop	2
R Rotor Mean Radius	.26 m	V_P Plenum Volume	15.0 m^3
U Mean Rotor Velocity	92.9 m/s	τ time constant	.0352 s^{-1}
B non-dimensional parameter	1.098	G non-dimensional parameter	.0236

Table 2. Parameters used in Greitzer's analysis.

4 RESULTS

4.1 Comparison of Model and Analytical Results for a Simple Pipe

A simple pipe is a good starting place for comparison of the finite element models and analytical results. A pipe *24* inches in length and *2* inches in diameter is used for this initial comparison. For the analysis, the one-dimensional model has twenty-four elements and the three-dimensional model has *5,971* elements. If the pipe is open on both ends, it obeys the pressure release boundary condition, and the natural frequency is calculated algebraically by $f_n = ic/2L$, where i is the mode number (*1, 2, 3…*), c is the speed of sound in air, and L is the length of the pipe. A comparison of the natural frequencies calculated analytically and by the one-dimensional and three-dimensional models are shown in table 3. Similarly for a pipe closed at one end and open at

Analytical Results (hz)	1D FE Model (hz)	3D FE Model (hz)
278.9	278.9	278.9
557.7	557.7	557.9
836.6	836.6	837.0
1115.5	1115.5	1116.4
1394.4	1394.5	1396.1

Table 3. Comparison of the natural frequencies of an open-open pipe calculated analytically and by FE models.

Analytical Results (hz)	1D FE Model (hz)	3D FE Model (hz)
139.4	139.4	139.4
418.3	418.3	418.4
697.2	697.2	697.4
976.0	976.1	976.6
1254.9	1255.0	1256.1

Table 4. Comparison of the natural frequencies of a closed-open pipe calculated analytically and by FE models.

the other, the natural frequencies are calculated from $f_n = ic/4L$. The results for this case are shown in table 4. The calculation time for the one-dimensional model is under a second, while the three-dimensional model calculation takes several minutes. The use of the three-dimensional model is somewhat excessive in this case, since the one-dimensional model is faster and appears to be more accurate with significantly fewer elements.

4.2 Comparison of Model and Analytical Results for a Volume-Choke-Volume

The small volume-choke-volume used in the proof of concept piping system is a symmetric volume-choke-volume with a volume diameter of *7.942* inches, a choke diameter of *2.047* inches, and equal volume and choke lengths of *6* inches. The Helmholtz frequency of the volume-choke-volume is calculated using one of the two equations mentioned previously, and by the one-dimensional and three-dimensional models. The one-dimensional model uses *20* elements and requires less than a second of computation time, while the three-dimensional model *2296* elements and requires just under one minute of computation time. Table 5 summarizes the volume-choke-volume Helmholtz frequencies as calculated by the two models, and the two equations presented previously. The equations calculate frequencies that are somewhat lower than those calculated by the finite element models, likely due to approximations made by the equations. The measured acoustic response of the complete piping system with the volume-choke-volume show that the system responds with frequencies somewhere between the two calculations.

4.3 Piping System Modal Analysis

The proof of concept piping system was simulated for four cases, one dimensional with and without the volume-choke-volume, and three dimensional with and without the volume-choke-

	General VCV formula	Symmetric VCV formula	1D FE Model	3D FE Model
Helmholtz frequency (hz)	117.9	129.4	99.6	94.1

Table 5. Comparison of the VCV Helmholtz frequencies calculated analytically and by FE models.

	1D Model		3D Model	
	With VCV	Without VCV	With VCV	Without VCV
Number of Elements	152	151	69515	7554
Number of Nodes	305	303	14799	2017
Element Size	.84 – 1 in	.85 – 1 in	.44 – 1.31 in	.41 – 1.22 in
VCV Helmholtz Frequency (Hz)	94 Hz 101 Hz	N/A	94 Hz 101 Hz	N/A
Plane Wave Cut-off Frequency (Hz)	983 Hz	1949 Hz	983 Hz	1949 Hz

Table 6. Proof of concept model parameters.

	Without VCV		With VCV	
	1D	3D	1D	3D
1	37.3	38.7	32.6	31.7
2	78.9	80.8	70.8	66.8
3	123.5	125.5	114.7	106.8
4	169.2	171.4	146.6	122.5
Difference	4%		8%	

Table 7. Summary of proof of concept piping system results.

volume. The parameters are summarized in table 6, and the results are summarized in table 7. The system's cutoff frequency for plane wave only propagation is *983* Hz with the volume-choke-volume, and *1949* Hz without. The three dimensional meshes from SolidWorks are shown in figure 13. Figure 14 shows the three-dimensional mode shapes for the first four modes of the proof of concept piping system with the volume-choke-volume, as predicted by the three-dimensional model, and figure 15 shows the same for the piping system without the volume-choke-volume. Figures 16 shows the one-dimensional mode shapes for the first four modes of the piping system with the volume-choke-volume, as predicted by the one-dimensional model, and figure 17 shows the same for the piping system without the volume-choke-volume. Without the volume-choke-volume, the system acts as a simple half wave resonator, since it is open at both ends. The color scales for all the three dimensional plots are the same, with dark red being the maximum and dark blue being the minimum, and are referenced to the highest amplitude mode shapes. Therefore, it can be seen that the modes of the system with the volume-choke-volume installed are of lower

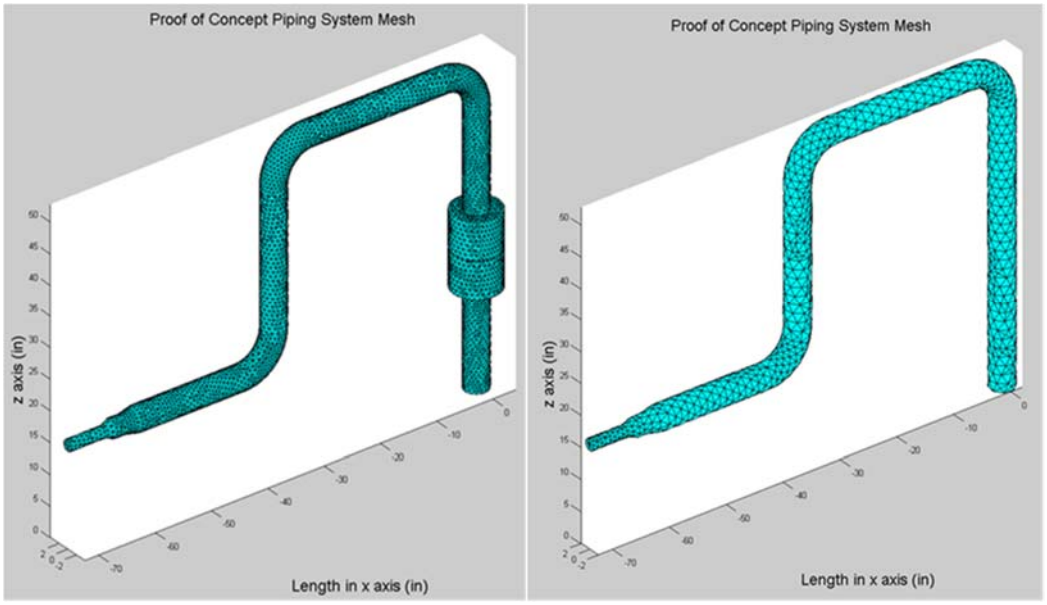

Figure 13. Finite element meshes of the proof of concept piping system.

amplitude than those without. The Helmholtz frequency of a volume-choke-volume is calculated by the formulae given by Wachel and Tison (Wachel, 1994), and the result is 101 Hz if the formula for a symmetric volume-choke-volume is used, and 94 Hz if the general equation is used. The difference is due to the use of the effective choke length in the general equation. Figure 18 shows a circumferential mode of the volume-choke-volume, a feature only capable with the three-dimensional model.

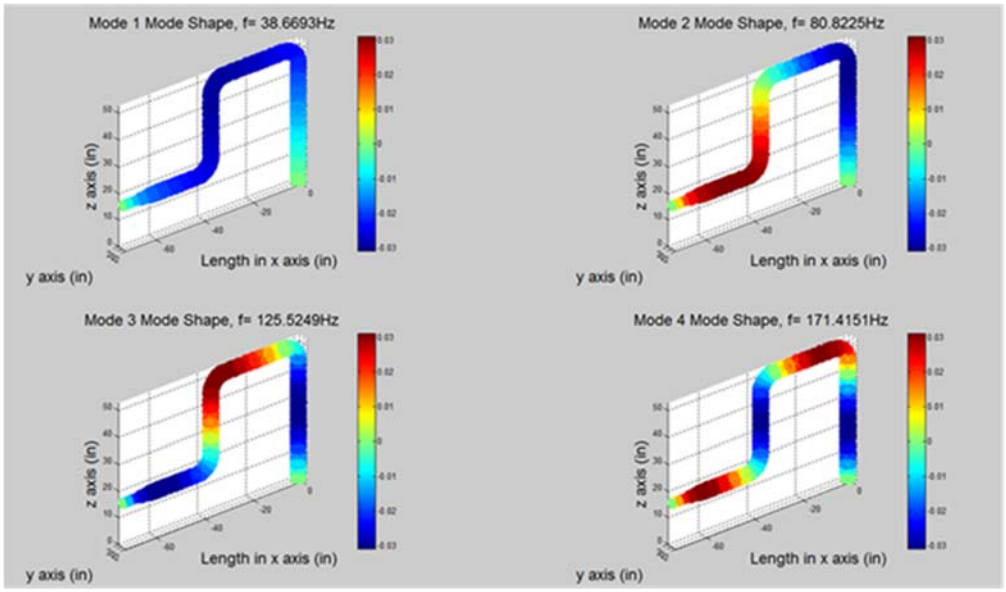

Figure 14. 3D scatterplots of the first 4 mode shapes of the 3D model without the VCV.

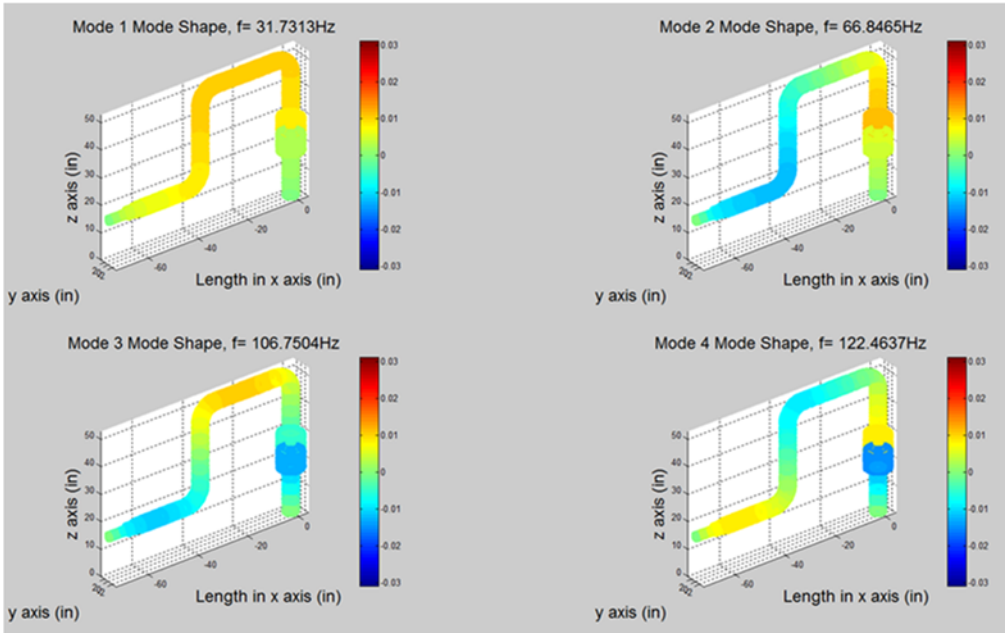

Figure 15. 3D scatterplots of the first 4 mode shapes of the 3D model with the VCV.

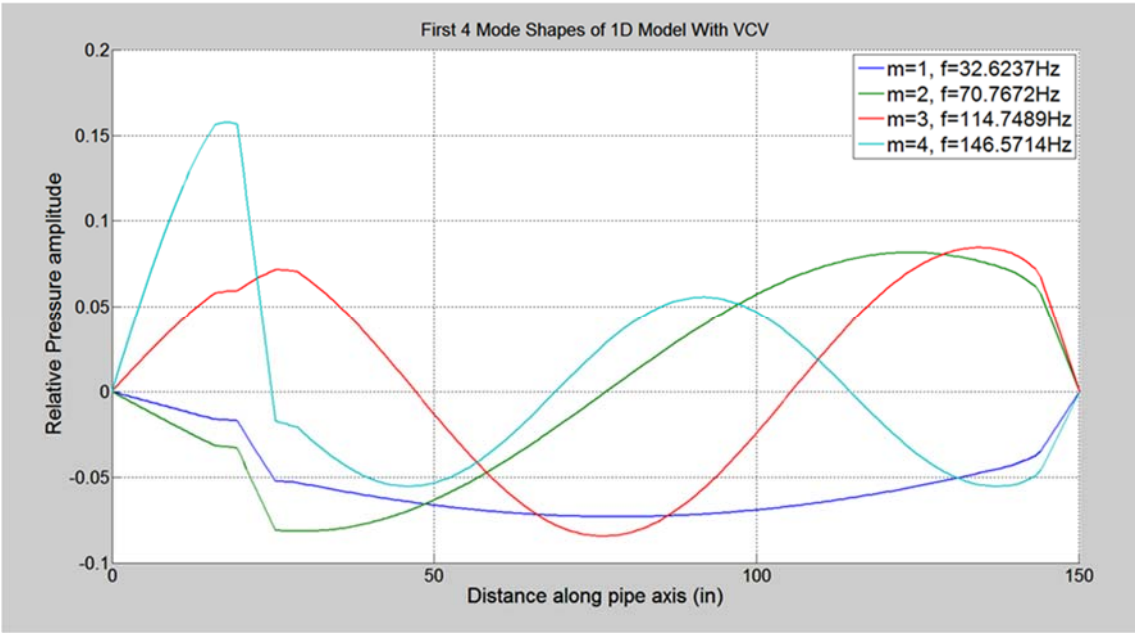

Figure 16. First 4 mode shapes of the 1D model with the VCV.

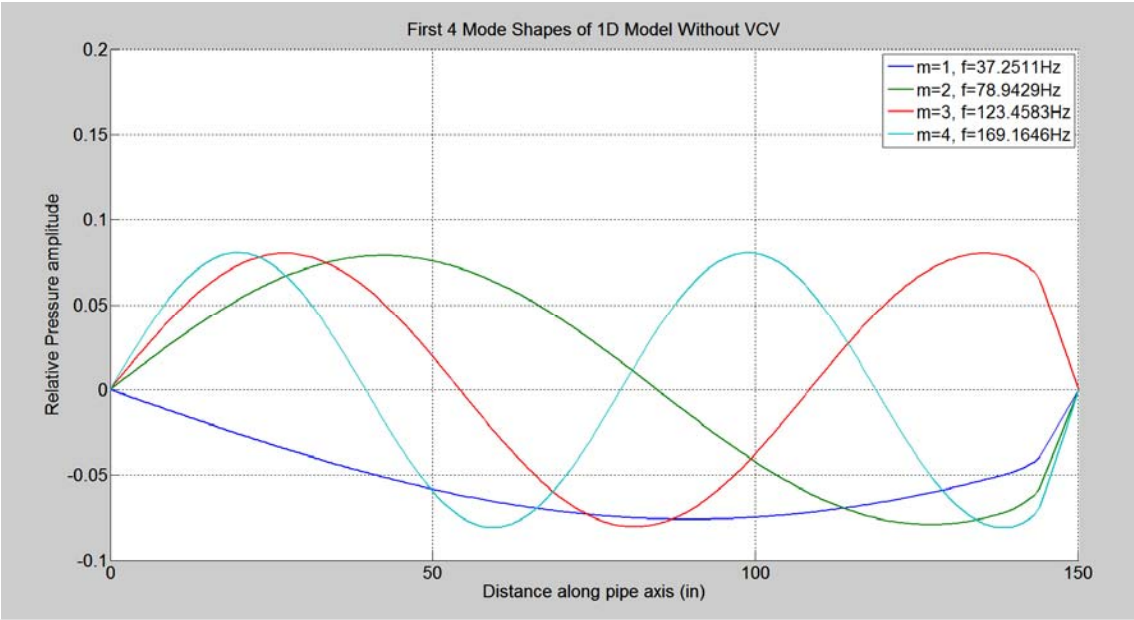

Figure 17. First 4 mode shapes of the 1D model without the VCV.

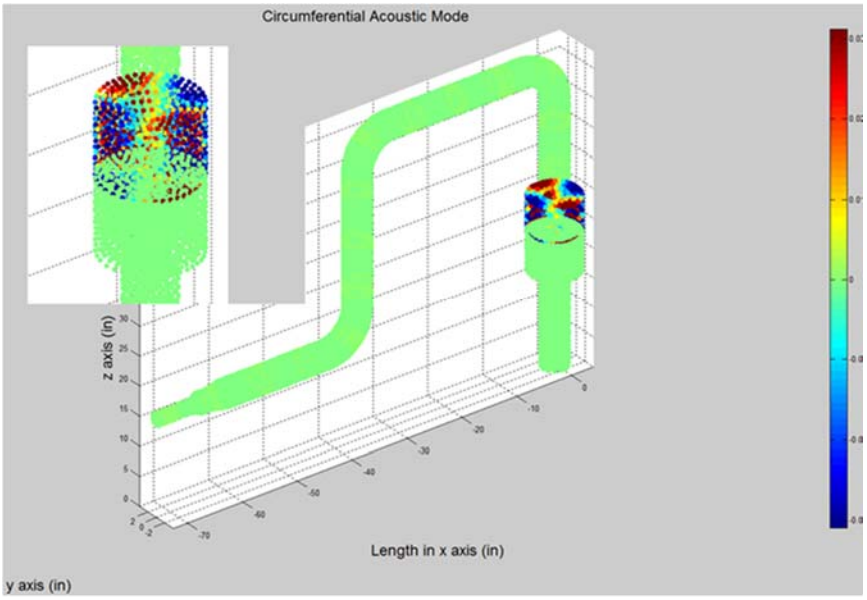

Figure 18. Circumferential mode shape as predicted by the 3D model.

The one dimensional and three dimensional simulation results correlate well, with less than 4% error between the two for the system without the volume-choke-volume, and generally less than 8% for the system with the volume-choke-volume (except for one value which had almost 18% error). The error here is due to the three dimensional code's ability to better model complex geometries. This is especially true in the model with the volume-choke-volume. Comparing the models to the experimental data also reveals a high level of accuracy in the model, at least in the case without the volume-choke-volume. Figure 19 shows the comparison of the experimental frequency domain data (blue lines) and the natural frequencies as predicted by the three-dimensional model (green bars) for the proof of concept piping system without the volume-choke-volume installed. The data recorded from the speaker end is in the top plot, and the data from the opposite end is in the bottom plot. Figure 20 shows the same comparison, but with the volume-choke-volume installed. The frequency spectrum data is in blue, the natural frequencies predicted by the one-dimensional model are represented by red bars, and the natural frequencies predicted by the three-dimensional model are represented by green bars. For the most part, sound pressure level peaks at both ends of the pipe line up well with the calculated natural frequencies. The inconsistency is likely due to some combination of background noise (in both the sound sense and

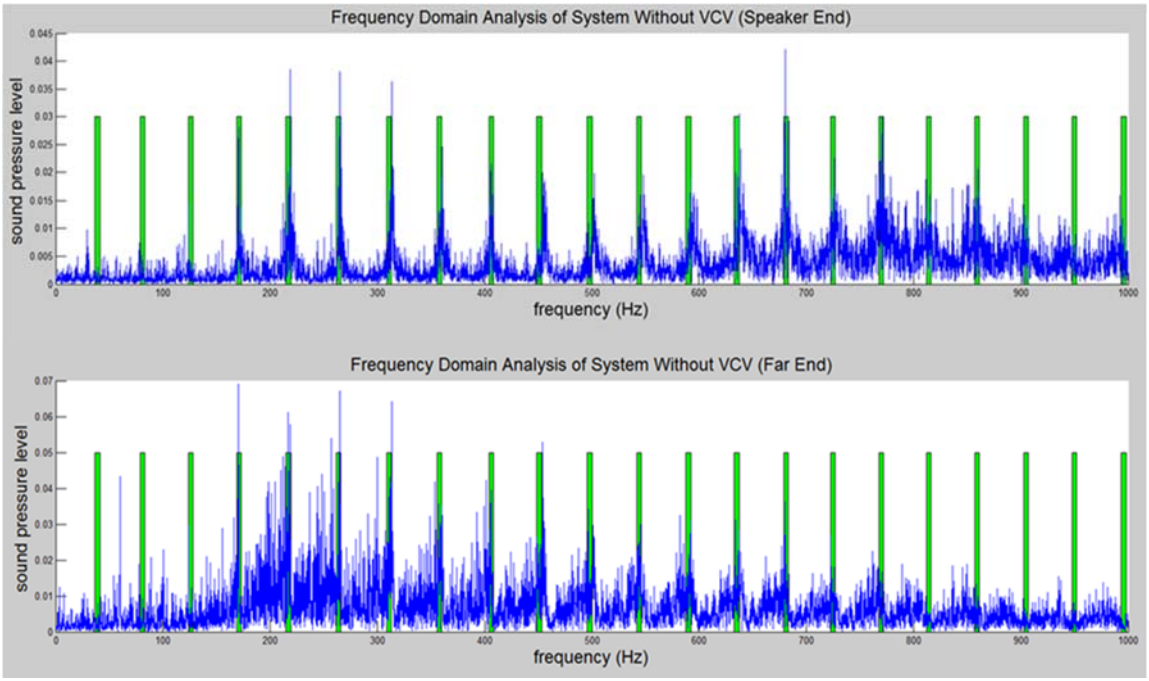

Figure 19. Frequency domain response of the proof of concept piping system without the VCV.

electrical sense), distortion of the white noise signal by the amplifier, and distortion of the sound pressure level signal between the microphones and computer. Also, at the far end of the pipe, there appears to be more noise in the signal, likely again due to background noise or the distance from the sound source. When the test was run on the system with the volume-choke-volume, the results were not as decisive. The data is much more scattered, due to the volume-choke-volume filtering the sound. In the few places where peaks occur in the frequency response, they are close to a predicted natural frequency, and appear to be only slightly closer to the three dimensional prediction than to the one dimensional prediction. There is a peak close to 100 Hz, which is close the Helmholtz frequency of the volume-choke-volume in the speaker end measurement, but it does not show in the measurement at the opposite end, indicating effective filtering.

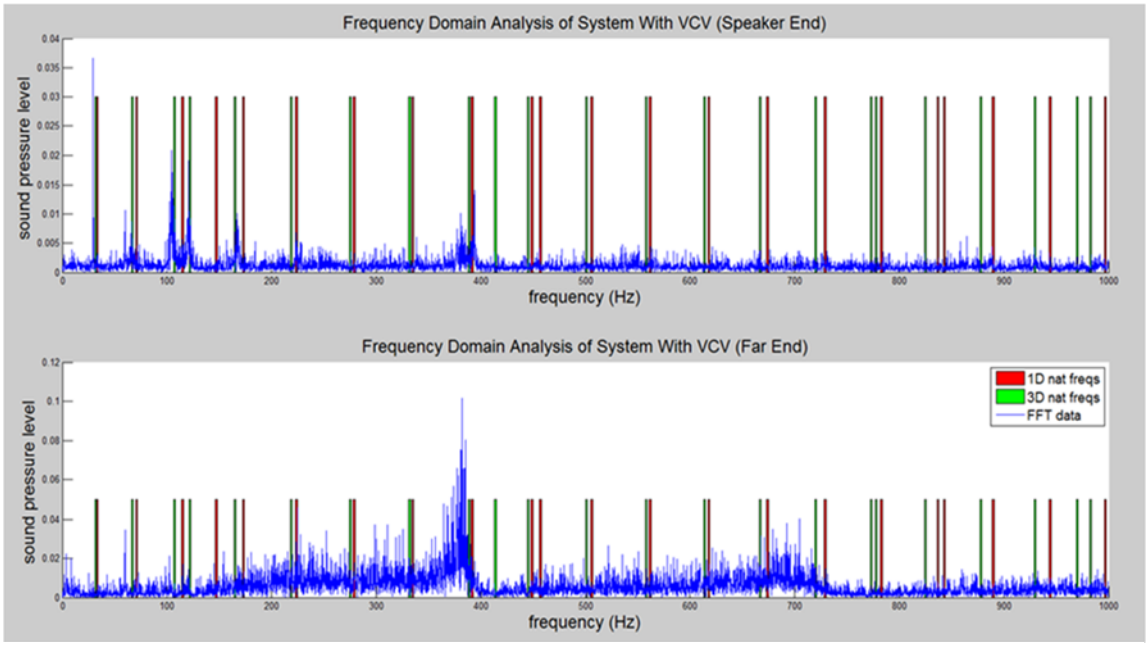

Figure 20. Frequency domain response of the proof of concept piping system with the VCV.

4.4 Combined Model

The reciprocating compressor model forces pressure pulses into the pipe by forcing gas through the valve. This interface is included in the finite element model as the time rate of change of mass flow rate. For a single cylinder, the forcing signal has a wave form similar to that shown in figure 21. When this type of wave form is applied directly to the pipe acoustic model, the result becomes unstable, causing a continuous increase in pipe pressure, instead of a reflected wave as is expected.

The transient solution to the combined model can be determined numerically, using a Runge-Kutta method. This analysis uses MATLAB ODE45. The solution to a simple system is shown in figure 22. The system uses a 10 cylinder reciprocating compressor with a compression ratio of 2:1 and a running speed of 1000 rpm. The reciprocating compressor discharges through a straight pipe (sized such that its natural frequency corresponds to the running speed of the reciprocating compressor) into a centrifugal compressor. The plot shows a close up view of the centrifugal

compressor map, with an expected operating point near where the two dotted lines meet. Oscillation about the steady state operating point is clear. The small amplitude of the oscillations is due to because the reciprocating compressor is not operating near the natural frequency of the pipe. This solution is only able to run for about half of one second before the solution begins to diverge.

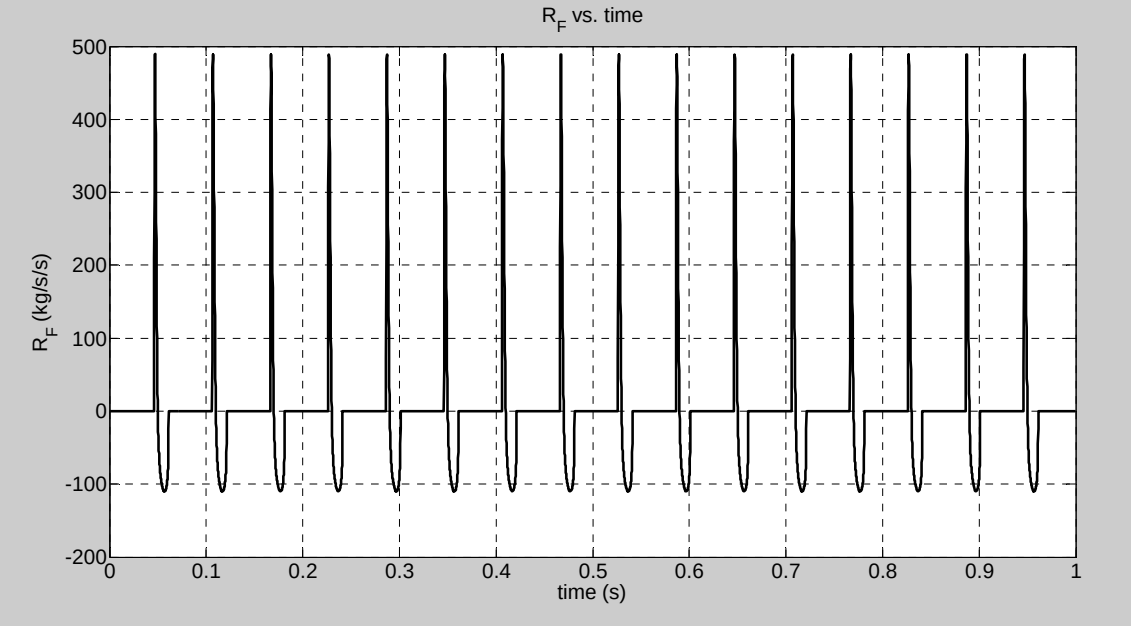

Figure 21. Forcing term waveform using a reciprocating compressor simulation.

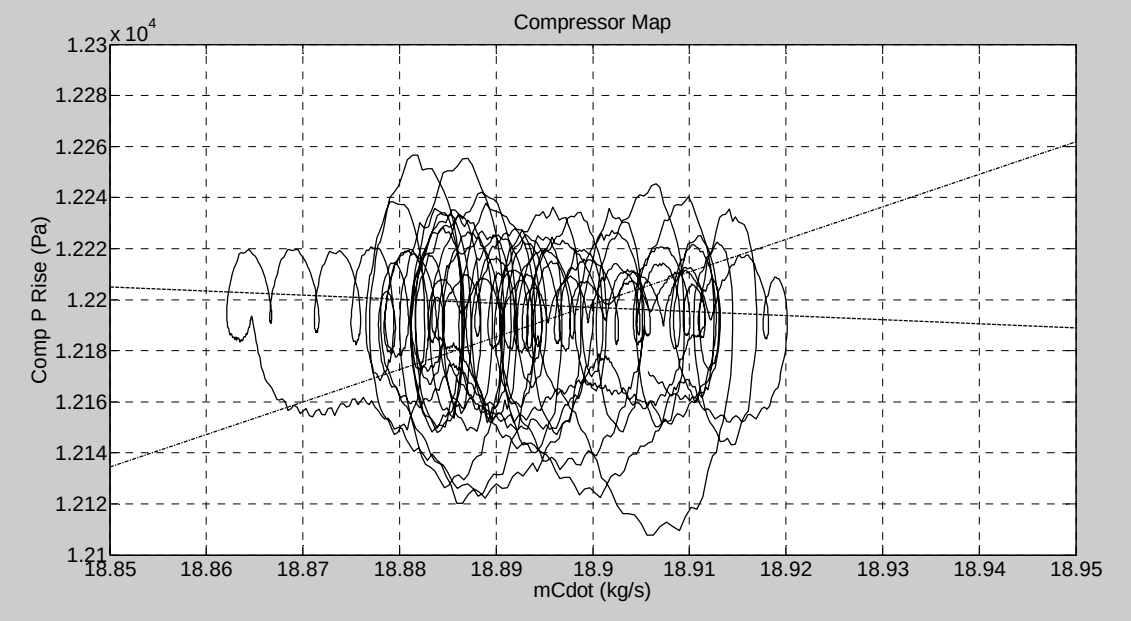

Figure 22. Combined system solution with reciprocating compressor coupled.

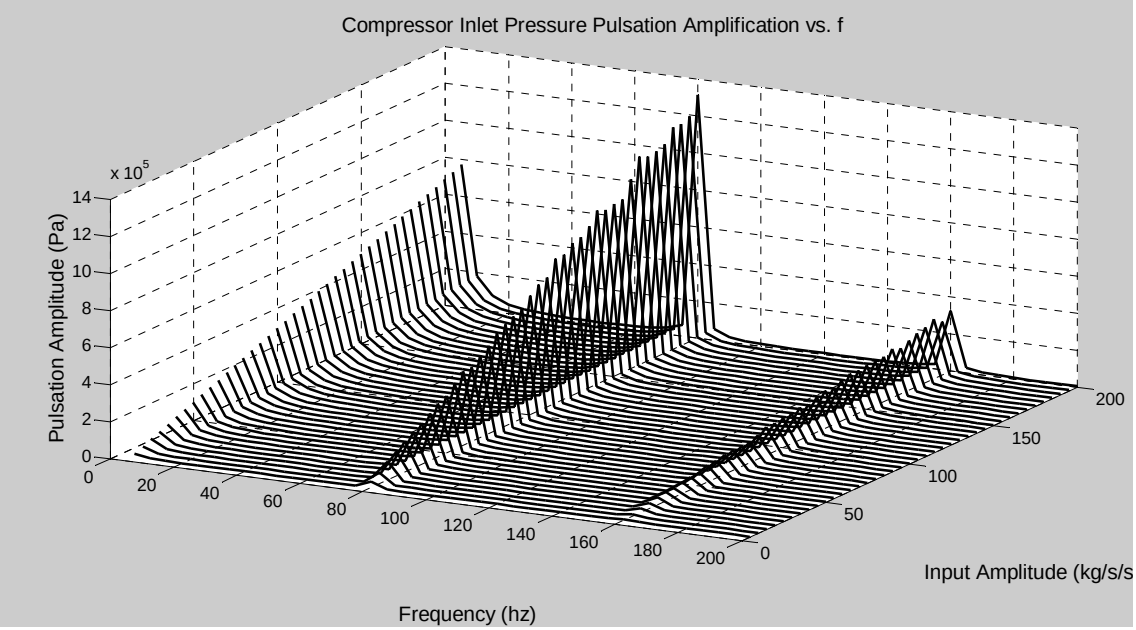

Figure 23. Compressor inlet pressure fluctuation for various input amplitudes & frequencies.

4.5 Parameter Study

To conduct the parameter study, the system simulation was modified by replacing the reciprocating compressor with a sinusoidal fluctuation as input, as discussed in the methodology section. This is done for two reasons. All numerical experiments are carried out with constant characteristics for the pipe, gas, and centrifugal compressor, while varying the input pulsation frequency (over a range of *5* to *200 Hz*, at *5 Hz* increments) and amplitude (over a range of *5* to *200 kg/s/s*, at *5 kg/s/s* increments). The pipe has length *2 m*, and diameter *0.2 m*. The natural frequencies of the pipe are *80.3 Hz*, *160.6 Hz*, and *240.9 Hz*. Because the pipe is a simple straight pipe with constant cross-section, the natural frequencies are easily calculated. The resulting pipe pressure fluctuations and compressor pressure and flow fluctuations were recorded for the various cases. Figure 23 is a waterfall plot of the pressure fluctuations at the centrifugal compressor suction. As expected, the pressure fluctuations peak at input frequencies corresponding to the natural frequencies of the pipe, and the fluctuation magnitudes increase with increasing input fluctuation amplitude. The values of the pressure fluctuation amplitude are not dependent on the pipe static pressure. This is because the pressure pulsation amplitudes are

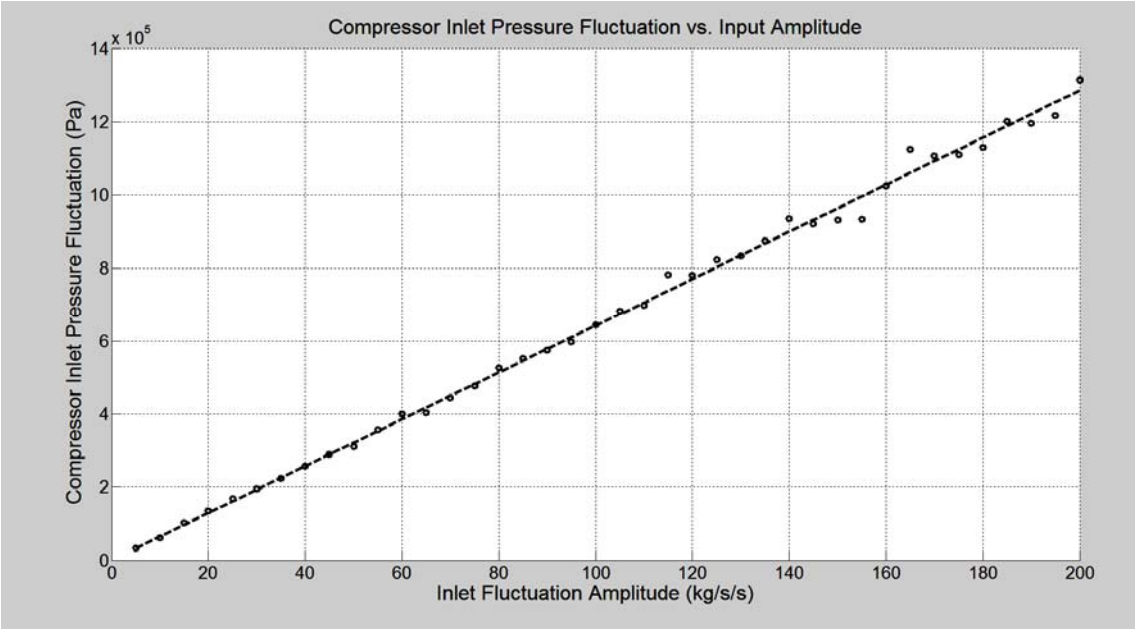

Figure 24. Compressor inlet pressure fluctuation versus input amplitude, with f = 80 hz.

determined by the pipe acoustics model, which only accounts for perturbations about the mean value (the mean value is assumed to be constant). The approximately linear relationship between the pipe pressure fluctuation amplitude is shown in figure 24 with a line of best fit. Figure 25 shows a waterfall plot of the centrifugal compressor mass flow rate fluctuations. The steady flow rate is dependent on the parameters of the compressor used in the Greitzer model and the compressor map. The fluctuation flow rate can be non-dimensionalized by dividing by the steady flow rate, as in figure 25. The fluctuation magnitude of the centrifugal compressor mass flow, however, is somewhat more erratic. Figure 26 shows the relationship with a line of best fit.

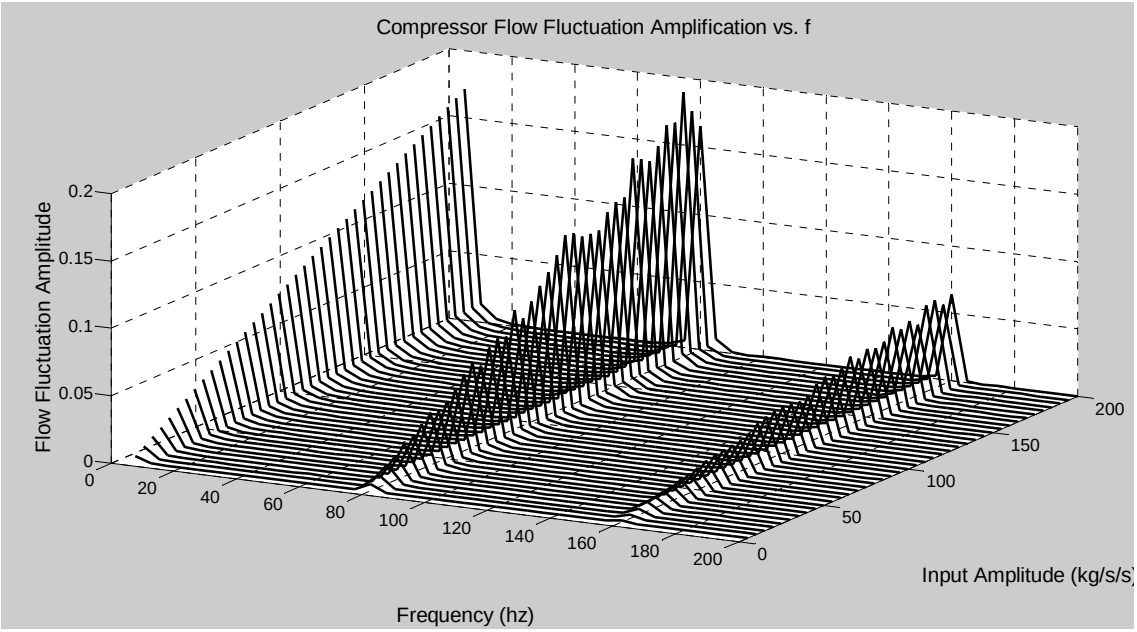

Figure 25. Compressor mass flow fluctuation (non-dimensional) for various input amplitudes and frequencies.

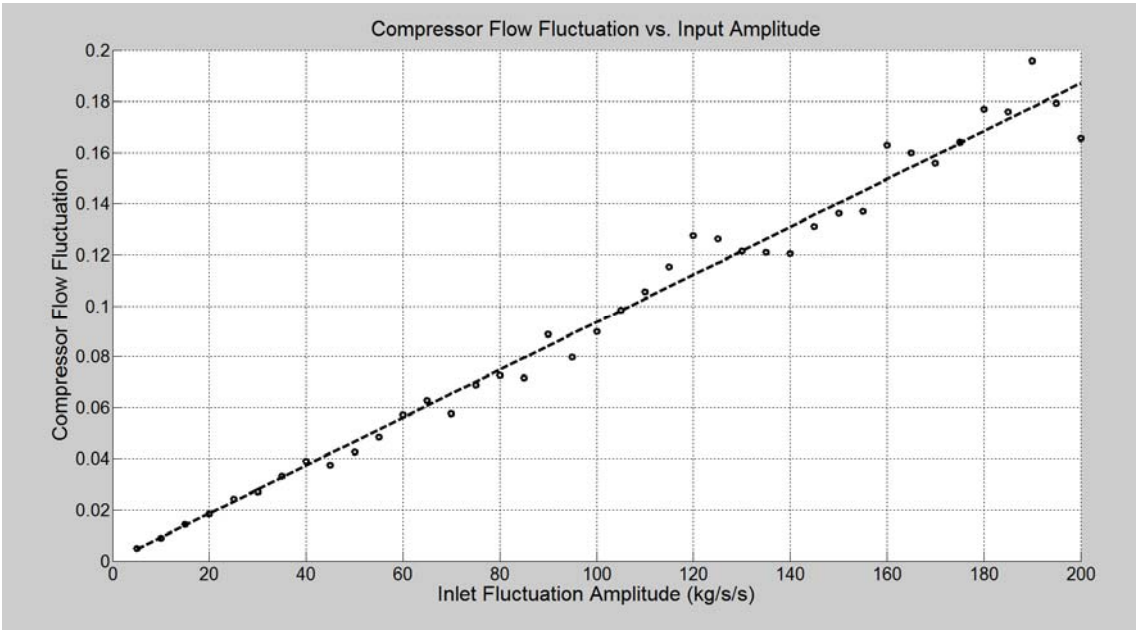

Figure 26. Non-dimensional compressor mass flow fluctuation versus input amplitude, with f = 80 hz.

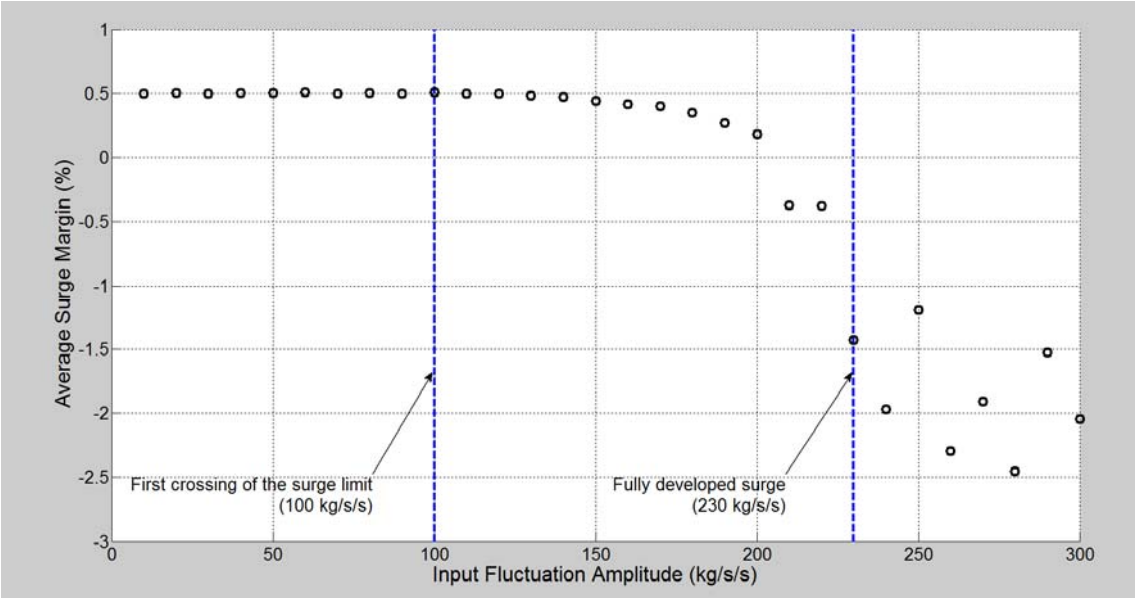

Figure 27. Surge margin versus input fluctuation amplitude at constant frequency.

4.6 Pulsation Induced Surge

It is hypothesized that a centrifugal compressor can be driven into surge by pulsations in the attached piping when the instability would not otherwise exist (the centrifugal compressor is operating at a stable operating point). To test this hypothesis with the model developed here, the same compressor system model as was previously analyzed in the parameter study is used. Here, the centrifugal compressor is initially operating in the stable portion of the centrifugal compressor map, but near the surge limit (*0.5%* surge margin). Then the system is analyzed over a variety of input amplitudes, *10* to *300 kg/s/s* at *10 kg/s/s* increments, with constant input fluctuation frequency set at *80 Hz*. The input frequency is chosen to be near the natural frequency of the pipe to maximize the resulting pulsation amplitude. A similar experiment is then run from the same initial condition, but this time the input fluctuation amplitude is held constant at *300 kg/s/s*, and the frequency is varied from *10* to *200 Hz* at *5 Hz* increments. For each of these experiments, the average surge margin for each case is calculated and plotted against the respective variable, input frequency or input amplitude, as shown in figures 27 and 28.

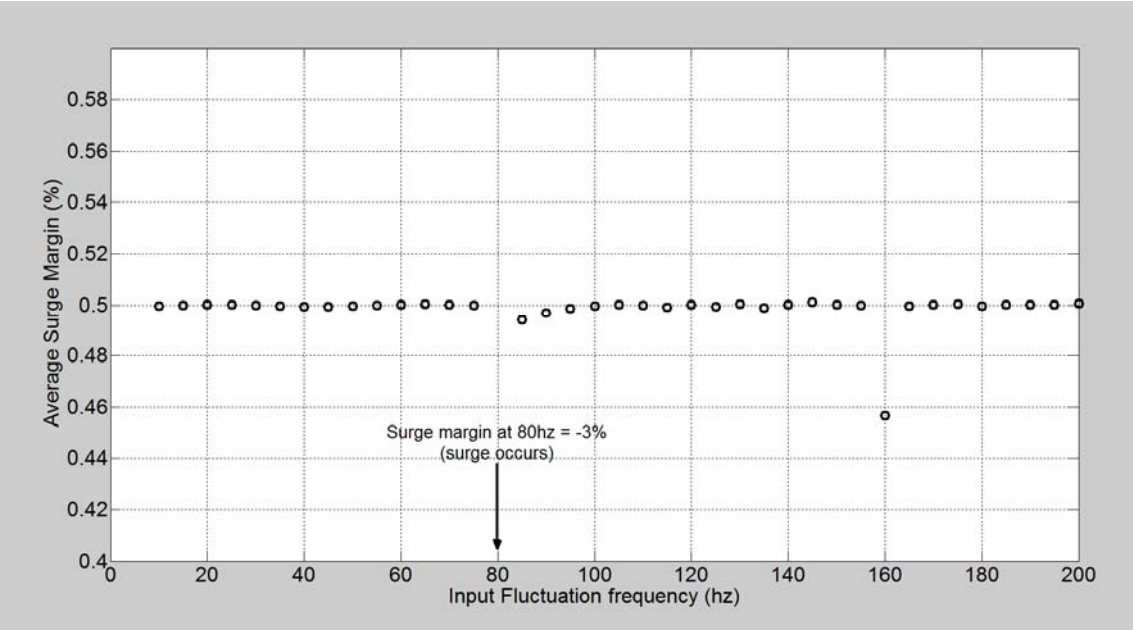

Figure 28. Surge margin versus input fluctuation frequency at constant amplitude.

In the analysis which varies input fluctuation amplitude at constant frequency (figure 27), the transition to surge is not a clean, abrupt switch. This appears to be because of the transient nature of the solution and the magnitude of the pulsations. For example, low amplitude input fluctuations which are not strong enough to push the compressor operating point over the surge limit cause the compressor to deviate from the operating curve, resulting in small oscillations about the stable operating point, and in the small fluctuations in average surge margin up to an input fluctuation amplitude of *90 kg/s/s*. As input amplitude increases, however, the resulting pulsations cause larger oscillations in the operating point, and drive the compressor over the surge limit, and then back into a stable operating range, as is the case for input fluctuation amplitudes between *100 kg/s/s* and *200 kg/s/s*. For these cases, the compressor crosses back and forth over the surge limit, even causing the average surge margin to be less than zero, without entering a full surge cycle. Hence, the average surge limit decreases, and even becomes negative, but the compressor does not fully enter surge. A small cycle mimicking the surge limit cycle develops as input fluctuation amplitude increases, however the transition to surge does not occur until the surge limit has been

exceeded enough to prohibit the pulsations from driving the operating point back to the stable region of the operating curve.

The analysis using constant input fluctuation amplitude and variable frequency (figure 28) shows a similar pattern as the previous analysis, except that now the transition to surge occurs when the input frequency is near the acoustic natural frequency of the attached pipe. At an input fluctuation frequency far from the pipe natural frequency, the pulsations cause a small oscillation about the compressor operating point, which remains small until the input frequency very nearly approaches the pipe acoustic natural frequency. The oscillation is strong enough to drive the compressor into surge only when the pipe acoustic natural frequency and input fluctuation frequency nearly exactly coincide. When the input fluctuation frequency is equal to the second harmonic of the pipe natural frequency, a large oscillation again develops. However, this oscillation is of smaller magnitude than as at the first harmonic, and while it does cause a small reduction on in average surge margin, it is not strong enough to drive the compressor into surge.

The compressor map and pipe acoustic pressure fluctuations for these situations are worth examining graphically. Figure 29 is for a case with an input frequency and amplitude of *65 Hz* and *95 kg/s/s* respectively. The surface plot on the left of figure 29 shows the normalized pipe acoustic pressure (the ratio of acoustic pressure to mean pressure) versus time and node location in the pipe. Here acoustic pulsations are small, with an amplitude less than *0.5%* of the mean pressure. This is expected due to the low magnitude of the forcing amplitude, and the difference between the forcing frequency and pipe natural frequency. The compressor map on the right figure is a close up of the operating point, showing the small oscillations resulting from the pipe acoustic fluctuations. The pressure rise values are non-dimensionalized by dividing by $\frac{1}{2}\rho U^2$ and the compressor flow rate by dividing by $\rho U A_C$, as is done in the Greitzer model. Figure 30 shows similar system results, with the same input frequency, but input amplitude is increased to the highest value tested, *300 kg/s/s*. The result of the increased input amplitude is an increase in magnitude of the acoustic piping fluctuations by about a factor of about three, to about 1.5% of the mean pressure. Also, the centrifugal compressor operating point oscillation amplitude increases, with both the pressure oscillation magnitude and mass flow rate oscillation approximately tripling.

Figure 31 shows results for the same initial input amplitude of *95 kg/s/s*, but with an input frequency of *80 Hz*, near the natural frequency of the pipe. The result is much larger pulsations in the pipe, up to *20%* of the mean pressure, shown in the pipe pressure surface plot, and a larger variation in compressor pressure and flow, as can be seen in the plot on the compressor map. In this case, the change in operating point is significant, and causes a reduction in surge margin. The oscillation is enough to reduce the surge margin to less than zero momentarily, but not enough to force the compressor into surge. Figure 32 shows the case where the input frequency is again *80 Hz*, but now the input fluctuation amplitude is *300 kg/s/s*. The pulsations occuring in the pipe are now staggering: greater than *50%* of the mean pipe pressure. These pulsations cause the compressor operating point to oscillate on the compressor map, crossing over and back across the surge limit, until the compressor finally enters the surge cycle, shown in the compressor map on the right hand side of figure 32. The fully developed surge limit cycle for the simulation takes several cycles to stabilize. This is likely due to the interaction with the piping system model, and the transient nature of the steady state centrifugal compressor rise due to the variation in compressor flow rate.

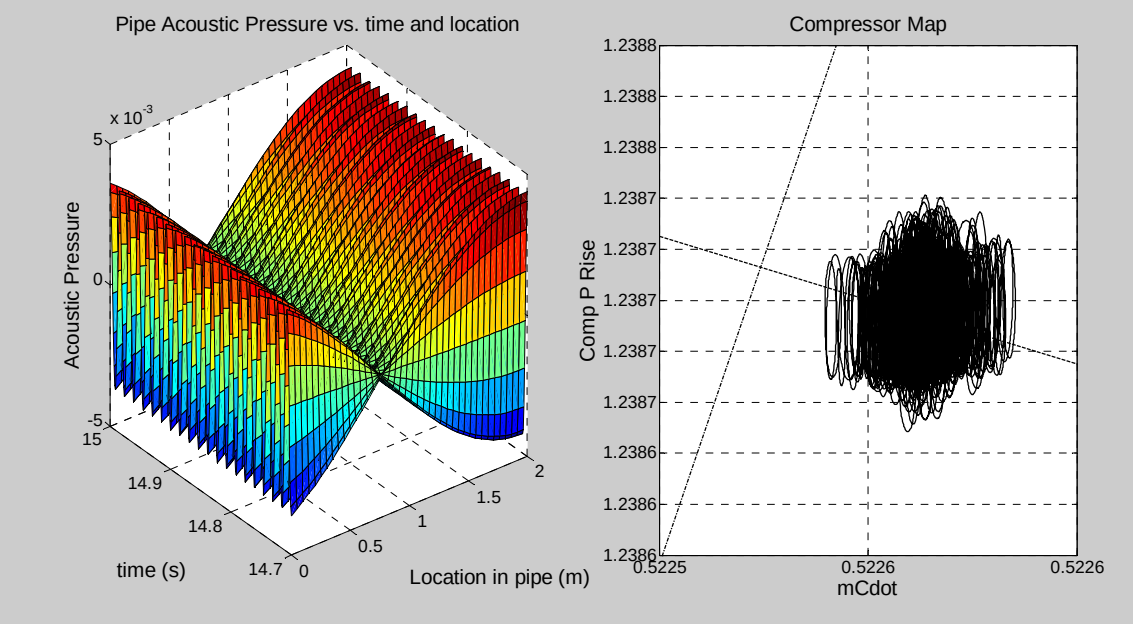

Figure 29. Non-dimensional pipe acoustic pressure vs. time and location (left) and compressor map (right) for R_0 = 95 kg/s/s & f = 65 Hz.

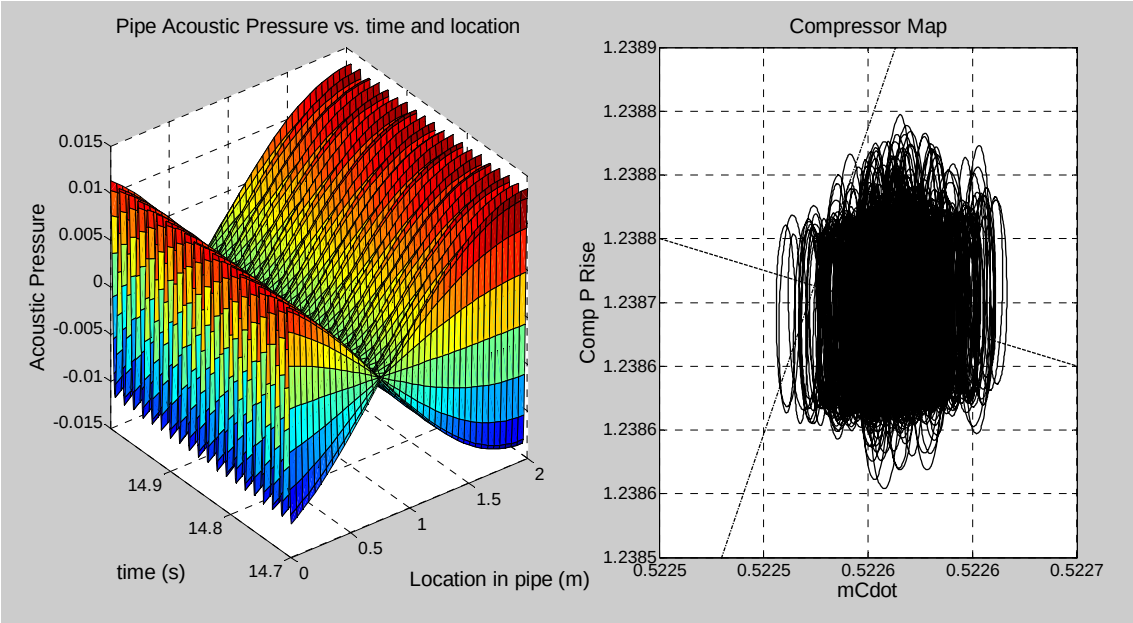

Figure 30. Non-dimensional pipe acoustic pressure vs. time and location (left) and compressor map (right) for R_0 = 300 kg/s/s & f = 65 Hz.

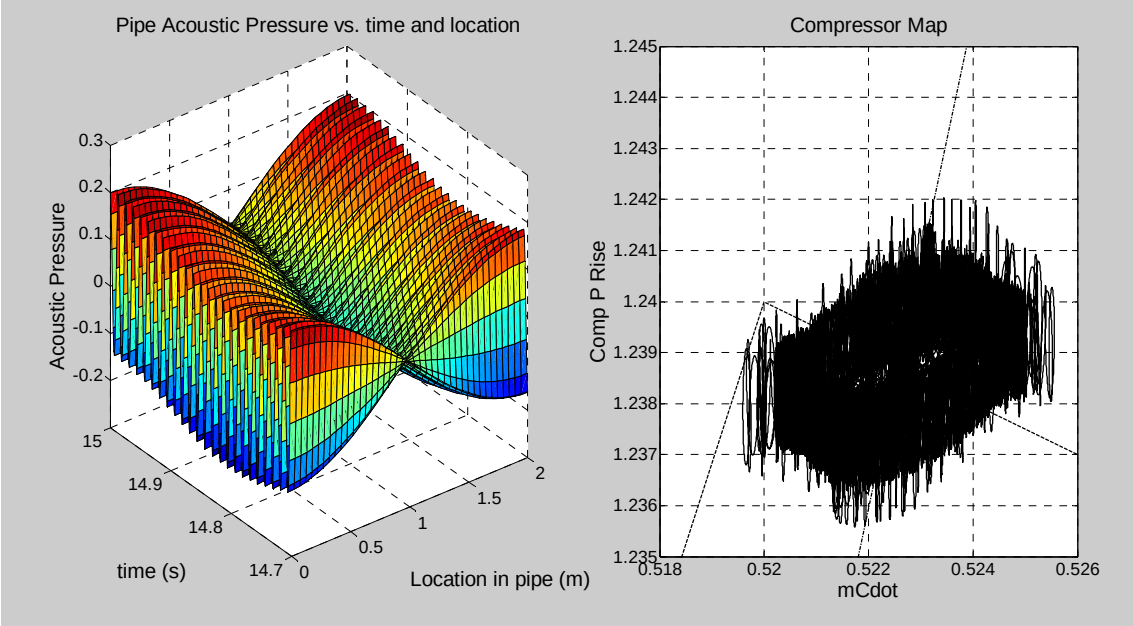

Figure 31. Non-dimensional pipe acoustic pressure vs. t and location (left) and compressor map (right) for R_0 = 95 kg/s/s & f = 80 Hz.

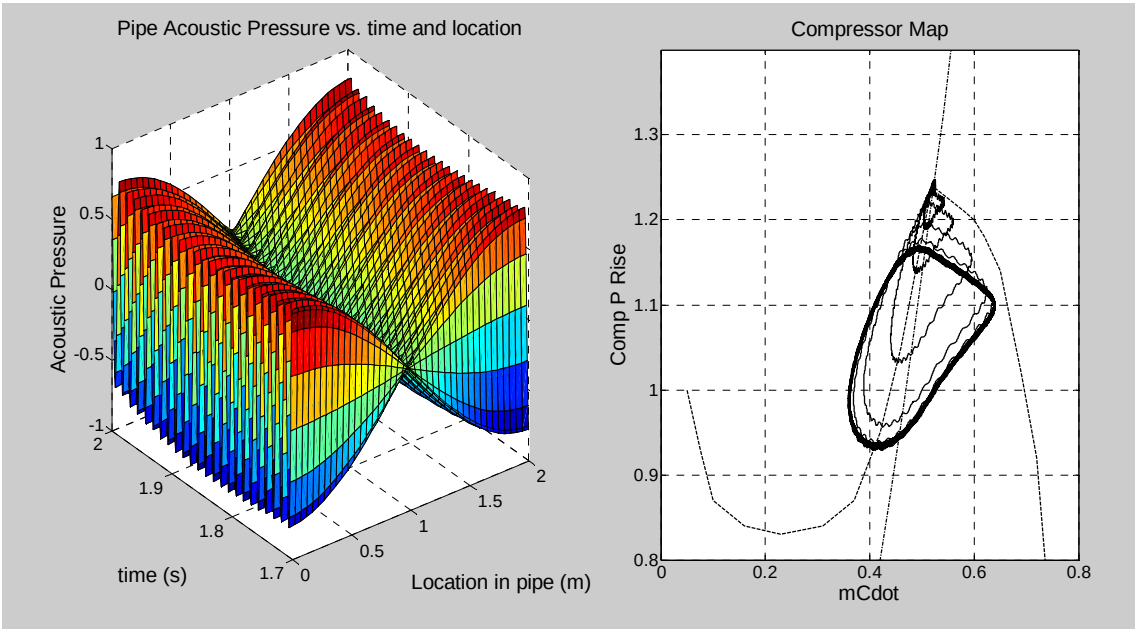

Figure 32. Non-dimensional pipe acoustic pressure vs. t and location (left) and compressor map (right) for R_0 = 300 kg/s/s & f = 80 Hz.

5 CONCLUSIONS

In this work, one-dimensional and three-dimensional finite element models were developed to simulate the acoustic response of pipelines using a discretization of the linearized wave equation, which allowed for equations for the mass and stiffness matrices to be derived. The elemental matrices for one dimensional quadratic elements and three dimensional tetrahedral elements were determined for use in the model, which can be assembled into system matrices. Then, a MATLAB code was written to calculate the acoustic natural frequencies and pressure modes by solving the eigenvalue equation resulting from modal analysis. Both the one dimensional and three dimensional models were found to calculate natural frequencies and mode shapes of simple pipes with a high degree of accuracy. For these simple arrangements, the one-dimensional model is more efficient, since it can perform the calculations much faster than the three-dimensional model, and with little error. More complex piping systems, especially when elements such as volume-choke-volumes are present, are better handled by the three-dimensional model. Complex geometries add error to the one-dimensional solution. Therefore, the three-dimensional model makes up for its slower computation time (due to having significantly more elements) with accuracy. The model was then coupled with a centrifugal compressor model, based on that developed by E.M. Greitzer, and a reciprocating compressor model for transient analyses. The acoustic model combined with the centrifugal compressor shows how the piping system interacts with the centrifugal compressor and affects its operating point. When the reciprocating compressor is combined with the pipe model, the discontinuity that occurs when the reciprocating compressor discharge valve opens tends to cause some numerical instability in the model. As a result, the combined model including the reciprocating compressor does not run reliably and often gives unexpected results.

A parameter study was conducted using the one-dimensional finite element system coupled with the centrifugal compressor model and a sinusoidal input replacing the reciprocating compressor. The input frequency and amplitude were varied over a variety of representative values, and the results were studied for their effect on pulsations. The results showed that the pulsations at the centrifugal compressor inlet and the fluctuations in centrifugal compressor mass flow rate were strongly and linearly affected by input amplitude. They were also affected by input frequency, but

increased as the input frequency approached the acoustic natural frequency of the pipe. These results support the hypothesis that the acoustic properties of the pipe will serve to increase pulsations in the piping system. Further numerical experiments were run with a reduced initial surge margin of *0.5%*. This set of experiments first ran the transient solution with input frequency held constant at the pipe's first acoustic natural frequency and varied input amplitude. Then input amplitude was held constant and input frequency was varied. Results from these experiments show that pulsations near the acoustic natural frequency have a significant effect on surge margin, and if they are strong enough, can drive the operating point over the surge limit. It was also found that if the centrifugal compressor is below the surge margin momentarily, the pulsations can pull the compressor back into the stable region before a surge cycle develops. Therefore, the in order for the pulsations to drive the centrifugal compressor fully into surge, the pulsations must push the operating point past the surge limit for enough time for a surge cycle to develop. In the case where surge did occur as a result of pressure pulsations, the initial operating point had to be very close to the surge limit (surge margin of *0.5%* or less), and the pulsations had to be astoundingly large (on the order of *50%* or more of the pipe mean pressure). It was also found that the surge cycle took several cycles to fully develop into its final limit cycle. This behavior is likely due to the interaction between the centrifugal compressor and piping system, and the fluctuations in compressor flow that cause transients in the steady state value of the centrifugal compressor pressure rise.

Additional work on this topic may include resolving the problems preventing the reciprocating compressor and centrifugal compressor from being directly coupled to the acoustic model simultaneously. This could include terms to account for the transient pipe mean pressure. To more accurately model all the complexities of pipe pressure fluctuations and flow, it might be necessary to develop a more sophisticated piping system model that includes mean pipe flow. The most thorough method to do this is might be a fluid dynamic model, for example. It might also be worthwhile to expand the Greitzer model to include more complex compressor geometry. Finally correlating the results of this work to experimental results would help refine and further validate the findings of this study.

REFERENCES

ANSYS Theory Reference Release 5.6. (1999). (P. Kohnke Ed. 11 ed.). Canonsburg, PA: ANSYS, Inc.

Arlett, P., Bahrani, AK, Zienkiewicz, OC. (1968). Application of Finite Elements to the Solution of Helmholtz's Equation. *Proceedings of the Institution of Electrical Engineers-London, 115*(12), 1762-1766.

Bathe, K. J. (1982). *Finite Element Procedures in Engineering Analysis*. Englewood Cliffs: Prentice-Hall.

Bermudez, A., Hervella-Nieto, L, Rodriguez, R. (1999). Finite Element Computation of Three-Dimensional Elastoacoustic Vibrations. *Journal of Sound and Vibration, 219*(2), 219-306.

Blackstock, D. (2000). *Fundamentals of Physical Acoustics*: John Wiley & Sons, Inc.

Brun, K., Kurz, Rainer. (2010). Analysis of the Effects of Pulsations on the Operational Stability of Centrifugal Compressors in Mixed Reciprocating and Centrifugal Compressor Stations. *Journal of Engineering for Gas Turbines and Power, Transactions of the ASME, 132*(7).

Cook, R., Malkus, David, Plesha, Michael, Witt, Robert. (2002). *Concepts and Applications of Finite Element Analysis* (4 ed.): John Wiley & Sons, Inc.

Craggs, A. (1976). A Finite Element Method for Damped Acoustic Systems: An Application to Evaluate the Performance of Reactive Mufflers. *Journal of Sound and Vibration, 48*(3), 377-392.

Craggs, A. (1985). A Note on the Theory and Application of a Simple Pipe Acoustic Element. *Journal of Sound and Vibration, 85*(2), 292-295.

Cyklis, P. (2010). Advanced Techniques for Pressure Pulsations Modeling in Volumetric Compressor Manifolds. *Journal of Vibration and Acoustics, 132*.

Damewood, G. (1983). Controlling the Effects of Pulsations and Fluid Transients in Industrial Plants [Seminar Notes] (A. P. D. Southwest Research Institute, Trans.). In S. A. P. D. Staff (Ed.), *SGA-PCRC Seminar*. Dallas, TX: Southern Gas Association.

Damewood, G., Nimitz, W. (1958). *Electo-Acoustical Analog for Pulsation Suppression and Control in Gas Compressor Stations*. Paper presented at the Short Course and Conference on Automation and Computers, The University of Texas, Austin, Texas.

Desmet, W., Vandepitte, D. (2002). *Finite Element Method in Acoustics.* Paper presented at the ISAAC13 - International Seminar on Applied Acoustics, Leuven.

Gladwell, G. (1965). *A Finite Element Method for Acoustics*. Paper presented at the 5th Congres International D'Acoustique, Liege.

Greitzer, E. M. (1976a). Surge and Rotating Stall in Axial Flow Compressors Part I: Theoretical Compression System Model. *Journal of Engineering for Power, Transactions of the ASME, 98*(2), 190-198.

Greitzer, E. M. (1976b). Surge and Rotating Stall in Axial Flow Compressors Part II: Experimental Results and Comparison With Theory. *Journal of Engineering for Power, Transactions of the ASME, 98*(2), 199-211.

Greitzer, E. M., Moore, F K. (1986). A Theory of Post-Stall Transients in Axial Compression Systems: Part II - Application. *Journal of Engineering for Gas Turbines and Power, Transactions of the ASME, 108*, 231-239.

Hansen, K. E., Jorgensen, P, Larsen, P S. (1981). Experimental and Theoretical Study of Surge in a Small Centrifugal Compressor. *Journal of Fluids Engineering, Transactions of the ASME, 103*, 391-395.

Hollauer, C. (2007). *Modeling of Thermal Oxidation and Stress Effects.* (PhD), Vienna University of Technology, Vienna, Austria.

Kagawa, Y., Yamabuchi, T, Mori, A. (1977). Finite Element Simulation of an Axisymmetric Acoustic Transmission System with a Sound Absorbing Wall. *Journal of Sound and Vibration, 53*(3), 357-374.

Kattan, P. (2008). *MATLAB Guide to Finite Elements: An Interactive Approach*: Verlag Berlin Heidelberg: Spring.

Kinsler, L., Frey, Austin, Coppens, Alan, Sanders, James. (2000). *Fundamentals of Acoustics* (4 ed.): John Wiley & Sons, Inc.

Kurz, R., White, R. C. (2004). Surge Avoidance in Gas Compression Systems. *Journal of Turbomachinery, Transactions of the ASME, 126*(4), 501-506.

Liu, B., Feng, J, Wang, Z, Peng, X. (2012). Attenuation of Gas Pulsation in a Reciprocating Compressor Piping System by Using a Volume-Choke-Volume Filter. *Journal of Vibration and Acoustics, 134*.

McMillan, G. K. (2010). *Centrifugal and Axial Compressor Control* (1 ed.). New York, NY: Momentum Press, LLC.

Moore, F. K., Greitzer, E M. (1986). A Theory of Post-Stall Transients in Axial Compression Systems: Part I - Development of Equations. *Journal of Engineering for Gas Turbines and Power, Transactions of the ASME, 108*, 68-76.

Petyt, M., Lea, J, Koopmann, G H. (1976). A Finite Element Method for Determining the Acoustic Modes of Irregular Shaped Curves. *Journal of Sound and Vibration, 45*(4), 495-502.

Toyama, K. R., Jr., P. W.; Dean, Jr., R. C. (1977). An Experimental Study of Surge in Centrifugal Compressors. *Journal of Fluids Engineering, Transactions of the ASME, 99*(1), 115-124.

Tweten, D., Nored, Marybeth, Brun, Klaus. (2008). *The Physics of Pulsations*. Paper presented at the Gas Machinery Conference.

van Helvoirt, J., de Jager, B. (2007). Dynamic model including piping acoustics of a centrifugal compression system. *Journal of Sound and Vibration, 302*, 361-378.

Wachel, J., Tison, JD. (1994). *Vibrations in Reciprocating Machiner and Piping Systems*. Paper presented at the 23rd Turbomachinery Symposium, College Station, TX.

Yoon, S. Y., Lin, Zongli, Goyne, Chris, Allaire, Paul E. (2011). *An Enhanced Greitzer Compressor Model with Pipeline Dynamics Included.* Paper presented at the American Control Conference, San Francisco, CA, USA.

APPENDIX A

The generic expressions for elemental acoustic mass and stiffness matrices are:

$$[M_e] = \frac{1}{c^2} \int_{Vol} [N][N]^T \, dV$$

$$[K_e] = \int_{Vol} [B]^T [B] dV \text{ , where } [B] = \begin{bmatrix} \frac{\partial}{\partial x} \\ \frac{\partial}{\partial y} \\ \frac{\partial}{\partial z} \end{bmatrix} [N]^T$$

For one-dimensional quadratic elements with constant length *L*, and nodes at points *0*, *L/2*, and *L*, the shape function reduces to:

$$N = \begin{bmatrix} \frac{2}{L^2}(\frac{L^2}{2} - \frac{3}{2}xL + x^2) \\ \frac{4}{L^2}(-xL + x^2) \\ \frac{2}{L^2}(-\frac{xL}{2} + x^2) \end{bmatrix}$$

Inserting the shape functions into the mass and stiffness matrix equations and integrating results in:

$$[M_e] = \frac{A}{c^2} \int_0^L [N][N]^T dx = \frac{AL}{30c^2} \begin{bmatrix} 4 & 2 & -1 \\ 2 & 16 & 2 \\ -1 & 2 & 4 \end{bmatrix}$$

$$[K_e] = A \int_0^L [B]^T [B] dx = \frac{A}{3L} \begin{bmatrix} 7 & -8 & 1 \\ -8 & 16 & -8 \\ 1 & -8 & 7 \end{bmatrix}$$

Where *L* is the length of the element and *A* is the cross-sectional area of the element (Cook, 2002).

For the three-dimensional model, the general expressions remain the same, and the shape functions are:

$$N_i = \frac{1}{6V}(\alpha_i + \beta_i x + \gamma_i y + \delta_i \mathrm{z}), \text{ with } 6V = \begin{vmatrix} 1 & x_1 & y_1 & z_1 \\ 1 & x_2 & y_2 & z_2 \\ 1 & x_3 & y_3 & z_3 \\ 1 & x_4 & y_4 & z_4 \end{vmatrix}$$

Here, each set of *x*, *y*, and *z* coordinates represent one node (corner) of the tetrahedral element. Integrating to find the element stiffness matrix results in (Kattan, 2008):

$$[K_e] = V[B]^T [B]$$

Where *[B]* is found from:

$$[B] = \begin{bmatrix} \frac{\partial}{\partial x} \\ \frac{\partial}{\partial y} \\ \frac{\partial}{\partial z} \end{bmatrix} [N]^T = \frac{1}{6V} \begin{bmatrix} \beta_1 & \beta_2 & \beta_3 & \beta_4 \\ \gamma_1 & \gamma_2 & \gamma_3 & \gamma_4 \\ \delta_1 & \delta_2 & \delta_3 & \delta_4 \end{bmatrix}$$

To find the set of coefficients for one of the shape functions, set:

$$[N_1] = \frac{1}{6V} \begin{bmatrix} 1 & x_1 & y_1 & z_1 \\ 1 & x_2 & y_2 & z_2 \\ 1 & x_3 & y_3 & z_3 \\ 1 & x_4 & y_4 & z_4 \end{bmatrix} \begin{bmatrix} \alpha_1 \\ \beta_1 \\ \gamma_1 \\ \delta_1 \end{bmatrix} = \begin{bmatrix} 1 \\ 0 \\ 0 \\ 0 \end{bmatrix}$$

To solve for the coefficients, Cramer's rule is employed. Therefore, it is necessary to find the determinant of the matrix on the left hand side, which works out to be 1:

$$\det\left(\frac{1}{6V} \begin{bmatrix} 1 & x_1 & y_1 & z_1 \\ 1 & x_2 & y_2 & z_2 \\ 1 & x_3 & y_3 & z_3 \\ 1 & x_4 & y_4 & z_4 \end{bmatrix} \right) = \frac{6V}{6V} = 1$$

Applying Cramer's rule results in:

$$\alpha_1 = \begin{vmatrix} x_2 & y_2 & z_2 \\ x_3 & y_3 & z_3 \\ x_4 & y_4 & z_4 \end{vmatrix}, \beta_1 = -\begin{vmatrix} 1 & y_2 & z_2 \\ 1 & y_3 & z_3 \\ 1 & y_4 & z_4 \end{vmatrix},$$

$$\gamma_1 = \begin{vmatrix} 1 & x_2 & z_2 \\ 1 & x_3 & z_3 \\ 1 & x_4 & z_4 \end{vmatrix}, \delta_1 = -\begin{vmatrix} 1 & x_2 & y_2 \\ 1 & x_3 & y_3 \\ 1 & x_4 & y_4 \end{vmatrix}$$

The process is repeated for the other three shape functions by setting the second element of the right hand side vector equal to one and the rest to zero, and so on. Once the sixteen coefficients have been calculated, *[B]* is found by:

$$[B] = \frac{1}{6V}\begin{bmatrix} \beta_1 & \beta_2 & \beta_3 & \beta_4 \\ \gamma_1 & \gamma_2 & \gamma_3 & \gamma_4 \\ \delta_1 & \delta_2 & \delta_3 & \delta_4 \end{bmatrix}$$

Then the element stiffness matrix is calculated from:

$$[K_e] = V[B]^T [B]$$

The mass matrix in the three-dimensional model is determined by transforming the elemental coordinates into a local coordinate system (Hollauer, 2007):

$$x = x_1 + (x_2 - x_1)\xi + (x_3 - x_1)\eta + (x_4 - x_1)\zeta$$
$$y = y_1 + (y_2 - y_1)\xi + (y_3 - y_1)\eta + (y_4 - y_1)\zeta$$
$$z = z_1 + (z_2 - z_1)\xi + (z_3 - z_1)\eta + (z_4 - z_1)\zeta$$

The normalized shape functions become:

$$N_1 = 1 - \xi - \eta - \zeta$$
$$N_2 = \xi$$
$$N_3 = \eta$$
$$N_4 = \zeta$$

The integrand becomes:

$$[M_e] = \frac{|J|}{c^2}\int_0^1 \int_0^{1-\xi} \int_0^{1-\xi-\eta} [N(\xi,\eta,\zeta)][N(\xi,\eta,\zeta)]^T \, d\zeta d\eta d\xi$$

Where the Jacobian matrix *[J]* is:

$$[J]=\begin{bmatrix} x_2-x_1 & x_3-x_1 & x_4-x_1 \\ y_2-y_1 & y_3-y_1 & y_4-y_1 \\ z_2-z_1 & z_3-z_1 & z_4-z_1 \end{bmatrix}$$

Performing the integral results in:

$$[M_e]=\frac{|J|}{c^2}\begin{bmatrix} \frac{2}{120} & \frac{1}{120} & \frac{1}{120} & \frac{1}{120} \\ \frac{1}{120} & \frac{2}{120} & \frac{1}{120} & \frac{1}{120} \\ \frac{1}{120} & \frac{1}{120} & \frac{2}{120} & \frac{1}{120} \\ \frac{1}{120} & \frac{1}{120} & \frac{1}{120} & \frac{2}{120} \end{bmatrix}$$

Therefore the *x*, *y*, and *z* coordinates of each node in the element must be known to calculate the Jacobian determine and subsequently the mass matrix.

To build the global matrices, the global coordinates matrix and the global connectivity matrix must be known. The global coordinates matrix specifies the global *x*, *y*, and *z* locations of each node, and therefore has 3 columns for the three-dimensional model (for *x*, *y*, and *z*) and one column for the one-dimensional model (*x* only), and *N* rows, where *N* is the number of nodes. The global connectivity matrix specifies the global node numbers that correspond to each local node number of the element. For the three-dimensional model, it has *4* columns (one for each node in every element), and in the one-dimensional model it has 3 columns. The number of rows in the connectivity matrix is equal to the number of elements. Once these matrices are known, an array *L* is created, which assigns a zero value to each node that has a fixed pressure, and a unique integer to each degree of freedom (pressure is variable). The user must specify where fixed pressures are located. Then a *J* array is created which has the same contents as the *L* array, except with locations where *L* has a zero value are thrown out. The result is that while *L* has a length equal to the number of nodes, *J* has a length equal to the number of degrees of freedom of the system, and each value is a distinct integer value. Next, the global matrices are initialized, each a square matrix with length equal to the number of degrees of freedom (length of *J*). To build the matrices, the program goes to the first element and calculates the local mass and stiffness matrices. Then the program looks

at each location in the local matrix and determines the node numbers corresponding to that location (*B(e,r)* and *B(e,s)*, where *e* is the number of the element in question, and *r* and *s* are the row and column numbers in question), determines if the node is a degree of freedom by comparing to the corresponding value of the *L* array (Non-zero values of both *L(B(e,r))* and *L(B(e,s))* corresponds to a degree of freedom), and if the node is a degree of freedom, the program adds the value from the local matrix into the global matrix corresponding to that degree of freedom (*K(L(B(e,r)),L(B(e,s)))* and *M(L(B(e,r)),L(B(e,s)))*). The program repeats this process for each location of the local matrix before moving on to the next element. Figure 33 illustrates the process for building the *L* and *J* arrays, and figure 34 shows the process for assembling the global mass and stiffness matrices. The result is the populated global mass and stiffness matrices.

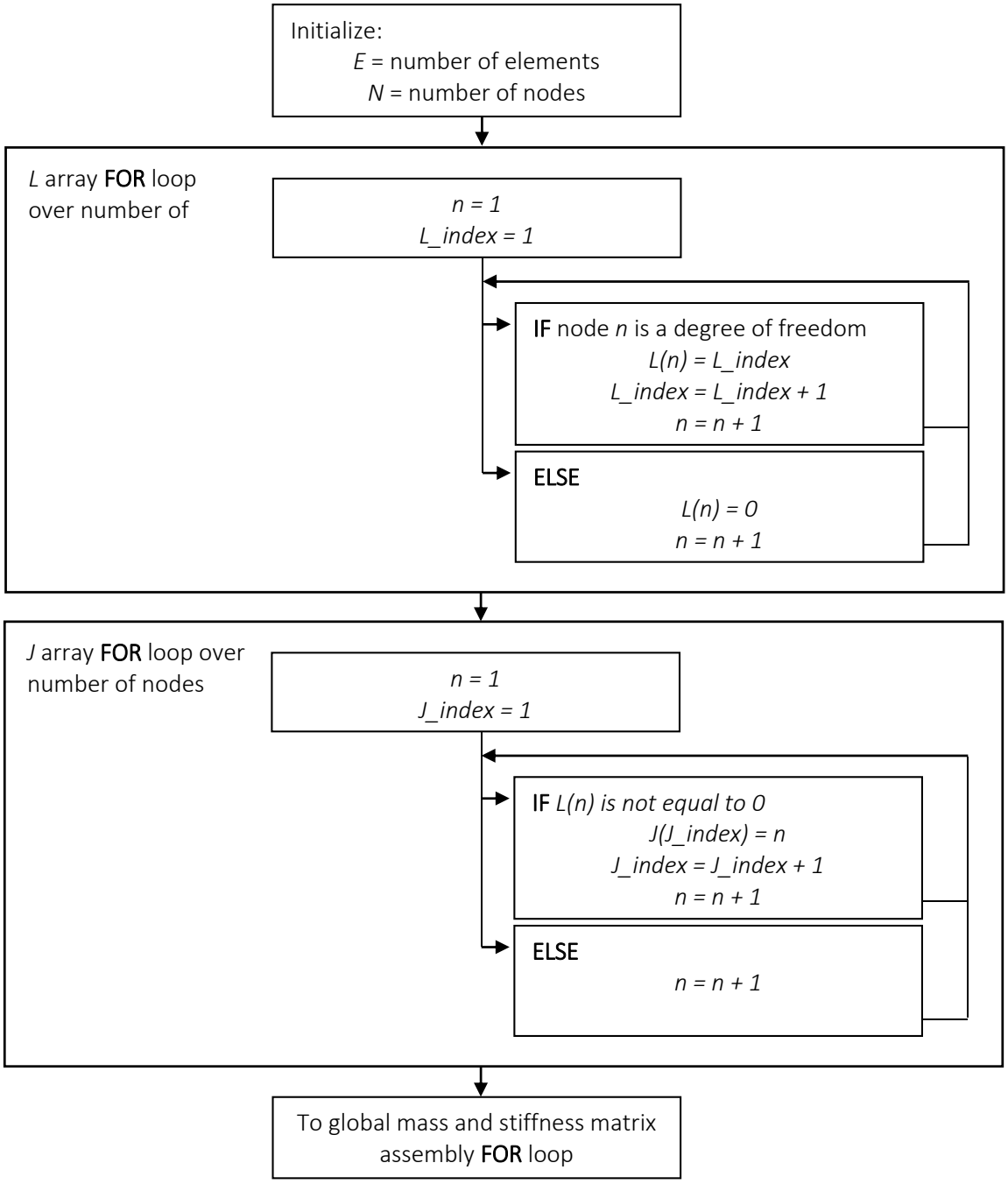

Figure 33. Procedure for building L and J arrays.

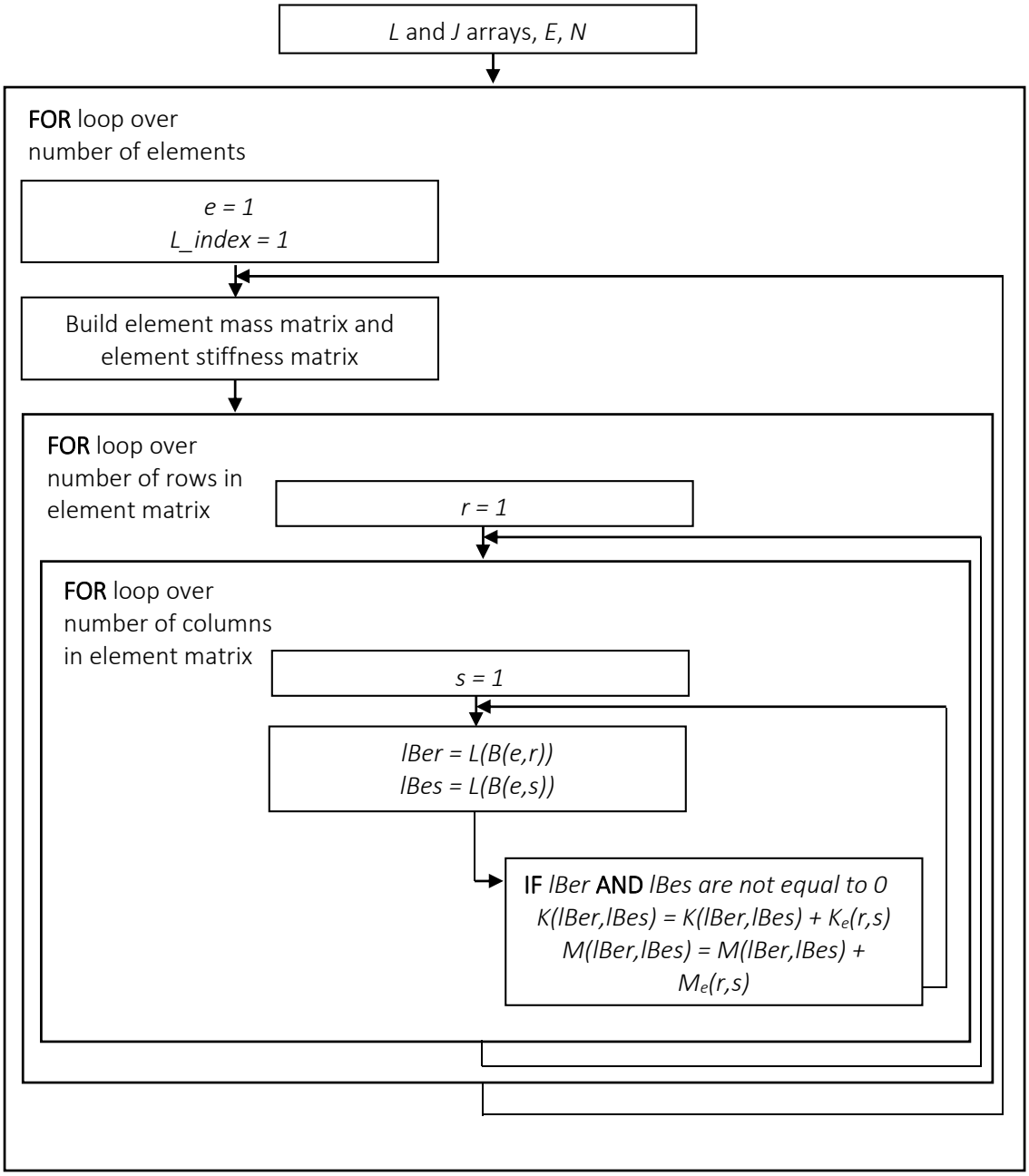

Figure 34. Procedure for assembling the global mass and stiffness matrices.